Representative profile model

a new physically-based model using slope unit for hazard assessment of colluvial landslides at large scale

Feng, Xiao; Du, Juan; Chai, Bo; Wang, Yang; Miao, Fasheng

DOI
10.1007/s10064-025-04677-2

Publication date
2025

Document Version
Final published version

Published in
Bulletin of Engineering Geology and the Environment

Citation (APA)
Feng, X., Du, J., Chai, B., Wang, Y., & Miao, F. (2025). Representative profile model: a new physically-based model using slope unit for hazard assessment of colluvial landslides at large scale. *Bulletin of Engineering Geology and the Environment*, *85*(1), Article 70. https://doi.org/10.1007/s10064-025-04677-2

Bulletin of Engineering Geology and the Environment (2026) 85:70
https://doi.org/10.1007/s10064-025-04677-2

ORIGINAL PAPER

Representative profile model: a new physically-based model using slope unit for hazard assessment of colluvial landslides at large scale

Xiao Feng[1,2] · Juan Du[3,4] · Bo Chai[3] · Yang Wang[1] · Fasheng Miao[1]

Received: 16 February 2025 / Accepted: 12 November 2025

Abstract

Physically-based model is an important method for refined assessment of landslide hazard at large scale. The traditional infinite slope model homogenizes the slope's structure and morphology, discretizing the slope into grid units and neglecting the interactions between different parts of the slope. However, slope units constitute the fundamental elements for stability analysis of natural slopes. Moreover, landslide bodies or slopes prone to landslides exhibit significant spatial heterogeneity. In order to realize the landslide hazard assessment in slope units, this study proposes a physically-based model called representative profile model (RPM). RPM takes the slope unit as the assessment unit and couples the slope surface morphology, Quaternary deposits thickness and ground water level. In order to represent the information of the slope unit within a single cross-section, the elevation range of the slope unit is divided with a uniform interval into some elevation segments. Each segment is assigned the average grid values of its respective elements. Then, a representative profile can be generated, consisting of ground surface, sliding surface, and ground water level. RPM also integrates the slices method and the Monte Carlo method to calculate the failure probability, allowing a physically-based hazard assessment in slope unit at a large scale. This study automates the process of RPM model through secondary development of ArcGIS. RPM model were applied in Tiefeng Township, Chongqing, China. The results validated by ROC curves and field investigation represent good performances, which could provide evidence of the potential of RPM for the landslide hazard assessment at regional scale.

Keywords Landslide hazard assessment · Large scale · Physically based model · Slope unit · ArcGIS secondary development

✉ Juan Du
dujuan@cug.edu.cn

Xiao Feng
fengxiao@cug.edu.cn

Bo Chai
chai1998@126.com

Yang Wang
wangyangcug@126.com

Fasheng Miao
fsmiao@cug.edu.cn

[1] Faculty of Engineering, China University of Geosciences, Wuhan 430074, China

[2] Water Resources Section, Faculty of Civil Engineering and Geosciences, Delft University of Technology, P.O. Box 5048, Stevinweg 1, Delft 2600 GA, The Netherlands

[3] School of Environmental Studies, China University of Geosciences, Wuhan 430074, China

[4] Centre for Severe Weather and Climate and Hydro-geological Hazards, Wuhan 430078, China

Introduction

Landslides are the most common and hazardous geological hazard in mountainous areas (Froude et al. 2018; Guzzetti et al. 2012; Eu et al. 2025; Caleca et al. 2025; Feng et al. 2024) and can occur in large numbers during the rainy season and cause property damage and loss of life. An accurate assessment of landslide hazard is necessary to minimize landslide risk (Van Westen et al. 2006; Petley 2012).

Landslide hazard assessment on a regional scale generally requires characterization of the spatial and temporal probability of landslide occurrence (Dehnavi et al. 2015; Miao et al. 2018&2022), and commonly used methods include matrix discriminant method and physically-based methods (Wang et al. 2020a, b; Brilli et al. 2025; Schilirò et al. 2018). The matrix discriminant method is one of the most commonly used methods for landslide hazard assessment, which usually superimposes rainfall probabilities on

Published online: 27 December 2025

the results of the susceptibility assessment to complete the hazard zoning. This method first analyses the spatial probability of landslide occurrence based on geological conditions or mathematical models (Guzzetti et al. 2000; Zhou et al. 2024) and then solves for the temporal probability of landslide occurrence by combining historical landslide inventories and events such as rainfall or earthquakes that induce landslides, and finally multiplying the spatial and temporal probabilities to obtain the landslide hazard (Lombardo et al. 2020). Currently, many studies are focusing on the comparison of susceptibility modeling methods based on machine learning (Chen et al. 2021; Xie et al.2021; Kim et al. 2021; Pradhan et al. 2023; Yang et al. 2023; Yang et al. 2024; Agboola et al. 2024), aiming to improve the accuracy of hazard evaluation by improving the accuracy of susceptibility assessment (Liu et al. 2021; Chang et al. 2023; Achu et al. 2023). However, such methods do not consider enough the physical mechanism of the landslide occurrence process, and only focus on the relationship between characteristic indexes and landslide occurrence, and the interpretability of their evaluation results is insufficient (Merghadi et al. 2020; Goetz et al. 2015; Yu et al. 2024; Vandromme et al. 2020). The accuracy of this method relies on a large amount of historical landslide data and extremely high data accuracy, and for this reason, a large number of studies have focused on landslide data logging (Xu et al. 2014; Al-Najjar et al. 2021; Woodard et al., 2025).

Currently, physically-based methods have also been introduced from single landslide stability analysis to landslide hazard assessment at a regional scale. This type of method has a clear physical-mechanical model and does not rely on historical landslide inventories which are rare and difficult to obtain worldwide (Marin et al. 2021; Liu et al. 2023; Thomas et al. 2023). The assessment results of physically-based models are highly interpretable because they can be verified by historical landslides (Peres et al. 2018; Ji et al. 2025).

The majority of physically-based models are based on the limit equilibrium method (LEM) or numerical simulation method (NSM) that use geotechnical constitutive models, simplifying the landslide or slope to a one-dimensional (1D) infinite slope, a two-dimensional (2D) profile, or a three-dimensional (3D) model and expresses landslide hazards by safety factors or failure probabilities (Michel et al. 2014; Van den Bout et al. 2021). In general, 1D infinite slope theory is adopted by most physically-based models applied to regional landslide hazard assessment. The ones that are being employed more frequently among these 1D physically-based models are SHALSTAB (Michel et al. 2014; Wang et al.2020), SINMAP (Lin et al., 2021), TRIGRS (Alvioli et al. 2016), and FSLAM (Guo et al. 2022; Durmaz et al. 2023; Cui et al. 2024a, b). The infinite slope model takes the grid as the fundamental unit to calculate the stability factor of each grid unit, without considering the interactions with surrounding units (Tran et al. 2018; He et al. 2021; Oguz et al. 2022). It allows for very fast calculations and is suitable for infinite plane slopes of similar soil thickness (Zhuang et al. 2017; Wu et al. 2015). However, this method is not suitable for high precision landslide hazard assessment as it ignores changes in slope surface and soil thickness (Viet et al. 2017). The 2D profile method is the preferred method for analyzing the stability of a single landslide, which is based on detail survey data and calculates the slope stability or failure probability using slice splitting and LEM. The method itself has been relatively mature while the high cost of obtaining landslide structure information is still the main reason that restricts the promotion of this method at a regional scale (Thiebes et al. 2014). 3D models are commonly employed for assessing the hazards of individual landslides due to the complex computational processes involved when using numerical simulation models (NSM) or improved LEM. Currently, Scoops 3D (Rashid et al. 2020; Liu et al. 2024a, b; Xue et al. 2024; Mergili et al. 2014; Palazzolo et al. 2021) and other models reduce the landslide's sliding surface to a straight plane or ellipsoid for computation, which is out of step with the landslide's actual circumstances and has a low calculation efficiency.

However, despite these advances, existing physically based models still face challenges in simultaneously capturing the three-dimensional geological complexity of slope units, representing spatial heterogeneity in soil thickness and topography, and maintaining computational efficiency for regional-scale mapping. To address this gap within the specific context of colluvial landslides, we propose the Representative Profile Model (RPM), a two-dimensional physically based framework that distills three-dimensional slope-unit information into a single, high-fidelity representative profile. RPM is designed primarily for slopes composed of loose Quaternary colluvial deposits, where the potential sliding surface typically develops near the interface between the colluvium and the underlying bedrock. The model generates multiple segmental lines across each slope unit to capture variations in colluvial thickness, groundwater level, and surface morphology, and then averages these data to construct a representative cross-section. This profile is analyzed using the residual thrust method coupled with Monte Carlo simulation to estimate the failure probability. By reconciling detailed geomechanical characterization with computational efficiency comparable to one-dimensional models, RPM provides a physically interpretable and spatially explicit tool for regional-scale assessment of colluvial landslide susceptibility and hazard, rather than for deep-seated or structurally controlled rockslides.

Methodology

Representative profile model

The Representative Profile Model (RPM) (Fig. 1) is a newly developed physically based model designed for regional-scale assessment of colluvial landslides. By abstracting the three-dimensional geological information of slope units into two-dimensional representative profiles, RPM enables efficient and physically interpretable slope stability analysis. The model integrates the digital elevation model (DEM), groundwater level, and Quaternary deposit thickness to determine the potential slip direction and segment each slope unit according to elevation. These segments are then used to construct two types of representative profiles: (i) a double-line profile, composed of the ground line and slip surface, which is used for landslide susceptibility assessment; and (ii) a triple-line profile, consisting of the ground line, slip surface, and saturation line, which incorporates groundwater level and is used for landslide hazard assessment. Through these profiles, RPM effectively captures both topographic relief and internal structural variability within each slope unit.

We have carried out a secondary development of ArcGIS using the C#.NET framework to build the Representative Profile Model (RPM) into an automated analysis program (Fig. 2). The graphical user interface (GUI) of RPM integrates all functional modules required for large-scale slope stability analysis. The software enables automatic extraction of essential data—including the digital elevation model (DEM), groundwater level, and Quaternary deposit thickness—within each slope unit, and performs slope segmentation, geometric parameter calculation, and representative profile generation in an integrated environment. Specifically, RPM includes (i) the slope unit segmentation and data processing modules (Fig. 2a, b,c),

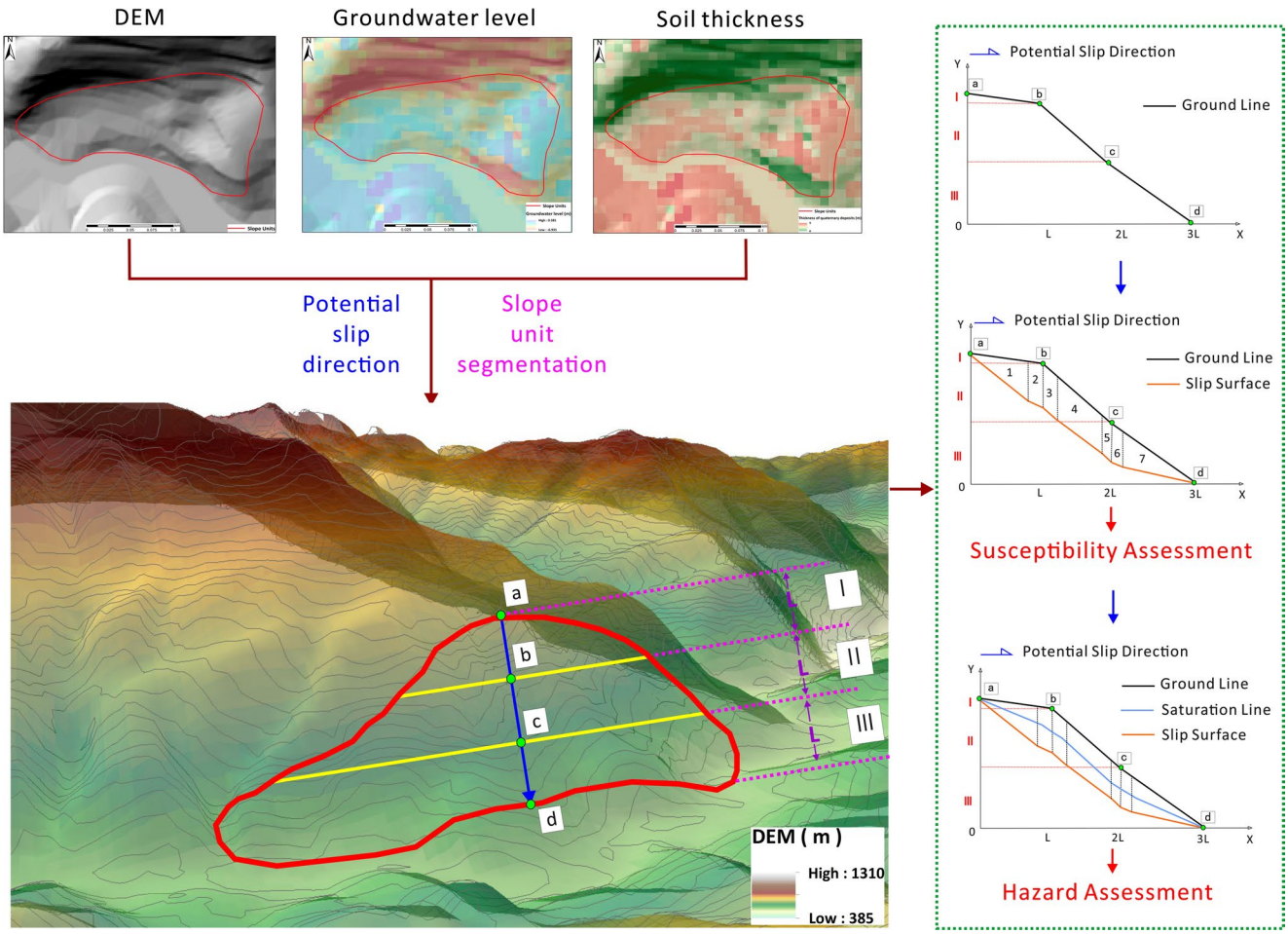

Fig. 1 Sketch map of RPM (Left: data inputs including DEM, groundwater level, and soil thickness; middle: extraction of potential slip direction and slope-unit segmentation; right: generation of double-line and triple-line representative profiles used for landslide susceptibility and hazard assessment.)

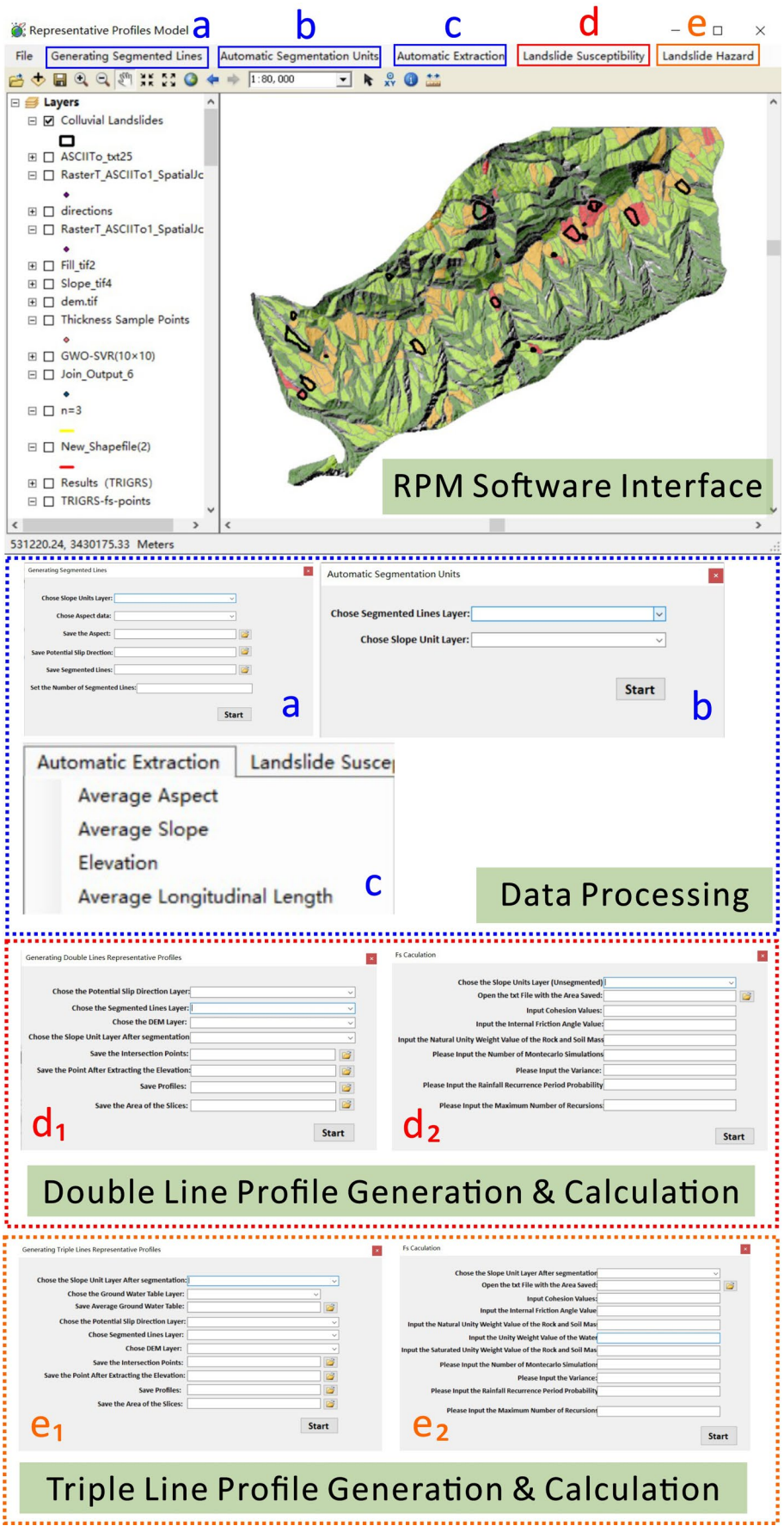

Fig. 2 Graphical user interface (GUI) of the RPM (**a–b**: interfaces for generating segmented lines and dividing slope units; **c**: interface for automatic data extraction and processing; $\mathbf{d_1}$–$\mathbf{d_2}$: modules for double-line profile generation and failure probability calculation; $\mathbf{e_1}$–$\mathbf{e_2}$: modules for triple-line profile generation and failure probability calculation)

which automatically generate segmented lines, divide slope units, and extract geometric attributes such as average aspect, slope, and elevation; (ii) the double-line profile generation and calculation modules (Fig. 2d_1, d_2), which exclude groundwater influence and are used for landslide susceptibility assessment; and (iii) the triple-line profile generation and calculation modules (Fig. 2e_1, e_2), which incorporate groundwater level and are applied for landslide hazard assessment. This design allows the entire modeling workflow—from data preparation to failure probability computation—to be completed efficiently and reproducibly within a single platform.

Figure 3 shows the overall workflow of the Representative Profile Model (RPM), which consists of four main stages. First, the required datasets—including slope units, digital elevation model (DEM), Quaternary deposit thickness, and groundwater level—are prepared as the fundamental inputs for regional slope stability analysis. From these datasets, additional terrain attributes such as aspect and slope gradient are derived to support hydrological and geometric analyses. Second, the slip direction of each slope unit is determined based on its average aspect, and the slope is subdivided into multiple elevation segments according to topographic relief. These steps define the geometric framework required for constructing representative profiles. Third, the intersection points between the slip direction line and elevation segments are used to generate the representative profiles. For each segment, the average soil thickness and groundwater level are computed, enabling the creation of double-line and triple-line profiles that respectively represent unsaturated and saturated conditions. Finally, the stability of each slope unit is evaluated using the limit equilibrium method (LEM) combined with the Monte Carlo method to estimate the failure probability. The resulting susceptibility and hazard maps provide a physically based assessment of landslide potential across the study area.

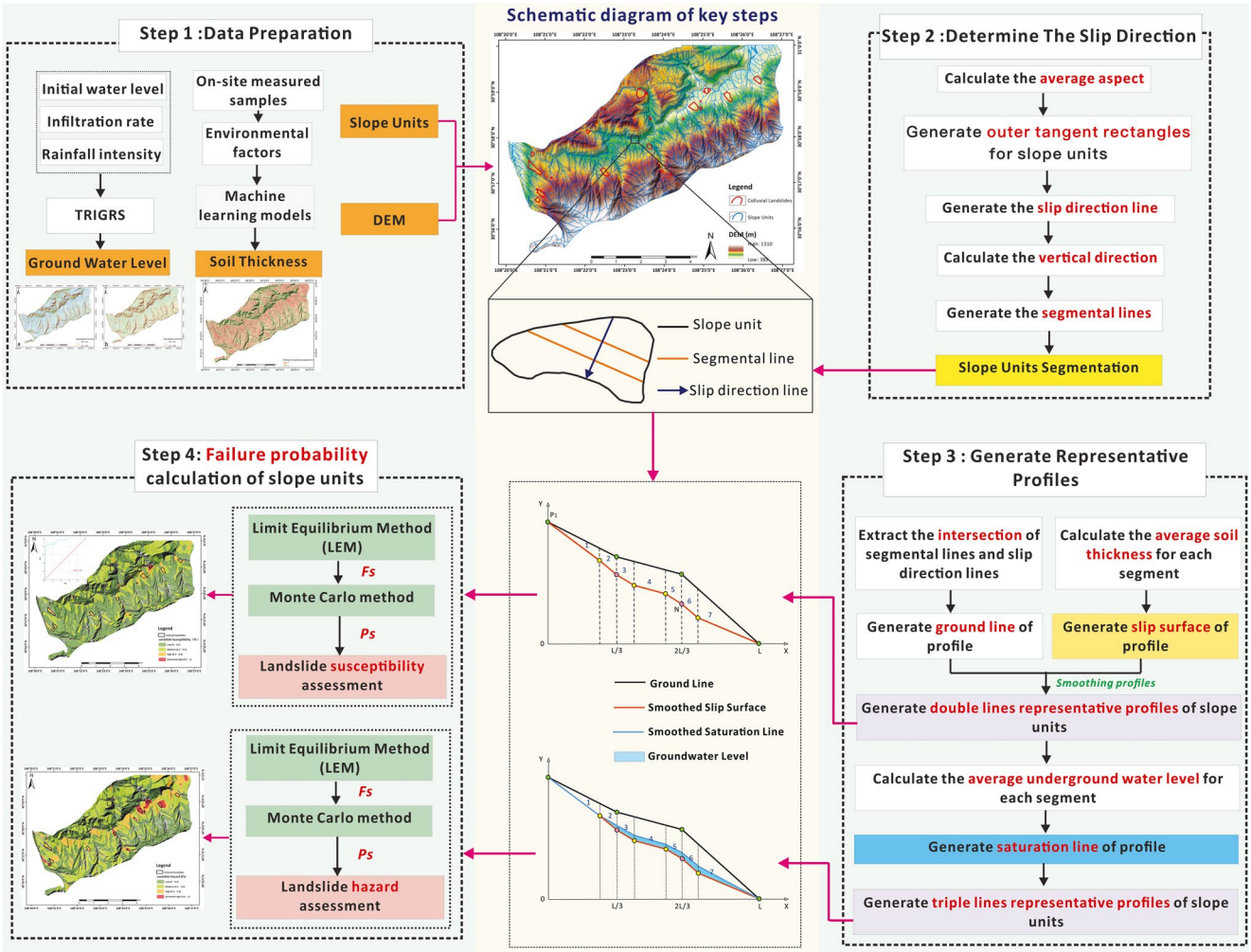

Fig. 3 Workflow of RPM

Slope units' segmentation and information extraction

The average aspect of a slope unit can, to some extent, represent its potential sliding direction. Once the potential sliding direction of a slope unit has been determined, there are numerous parallel potential sliding lines in the internal space (Fig. 4b). The profile of RPM should be obtained from the most representative potential slip direction line, which sets a constraint on the potential sliding line's spatial placement inside the slope unit. The potential sliding direction lines are generated through the following way in the automated program we developed for RPM:

1. Calculate the average of the aspect values for all raster within each slope unit.
2. Create an average aspect line EF along the slope unit's average aspect, and then create an enclosing rectangle ABCD of the slope unit (Fig. 4a), with the short side perpendicular to EF.
3. Join the midpoints of the lines AB and CD, MN, to generate the slope unit's representative profile line (Fig. 4b).

The infinite slope model assumes the ground line and slip surface are two parallel straight lines, ignoring the slope's true topographic relief. RPM proposed in this paper divides the slope unit into several segments by constructing segment lines, so that the profile shapes of different height zones of the slope unit can be accurately characterized. In theory, the more segmental lines there are, the closer the representative profile is to the actual slope shape (Fig. 5). The segmental lines are constrained by the following requirements: (i) they are perpendicular to the potential sliding direction lines; (ii) they are located within the slope unit and intersect the slope unit boundary; and (iii) The number of segment lines is n. The intersection of the segment lines with the potential sliding direction lines should divide the potential sliding direction lines equally into $n+1$ segments.

Once the slope units have been segmented, several pieces of information need to be extracted from each segment to provide the necessary data for the subsequent generation of the representative profiles. The information extracted in this step are mainly the average thickness of the Quaternary deposits, the average depth of ground water, and the average longitudinal length in each segment. The average thickness and depth of ground water are extracted from a raster-based mapping of the Quaternary deposits thickness and the ground water depth. The average longitudinal length is the distance between the intersection of the segmental line and the potential slip direction line.

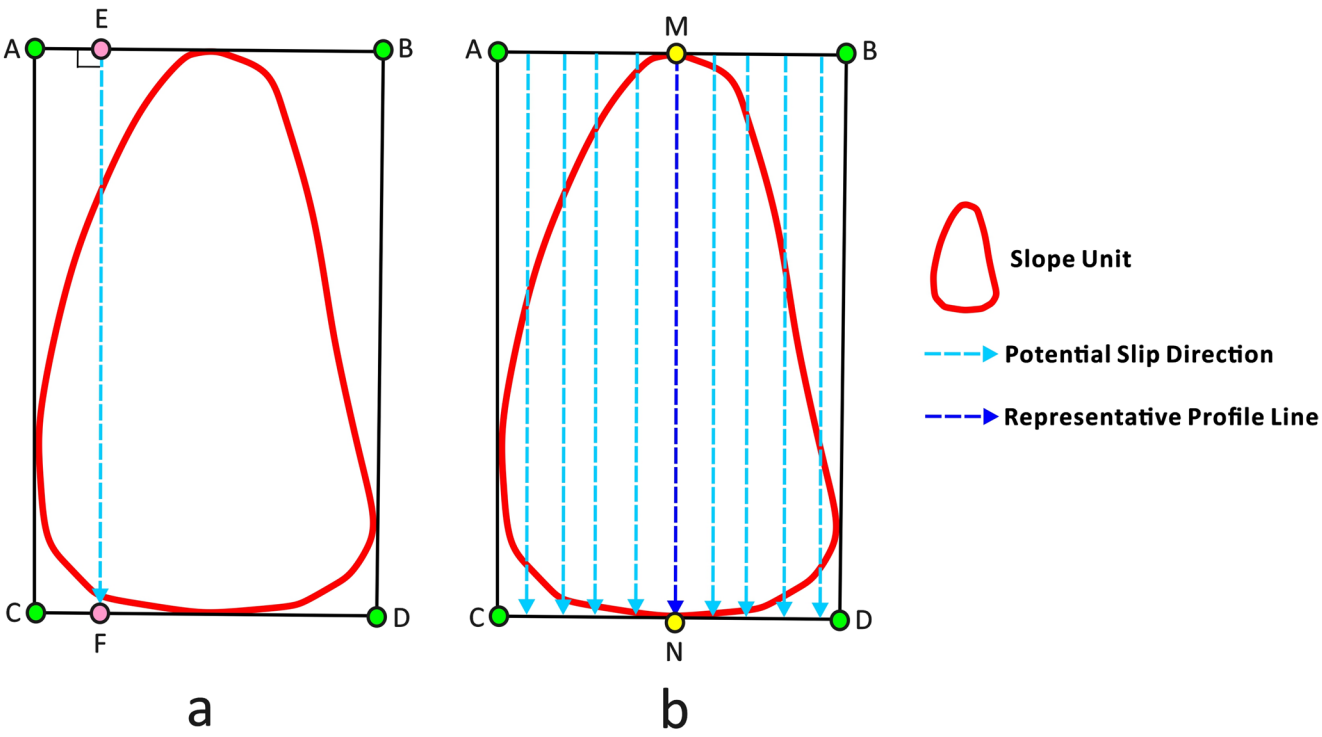

Fig. 4 Determining the position of the representative profile line

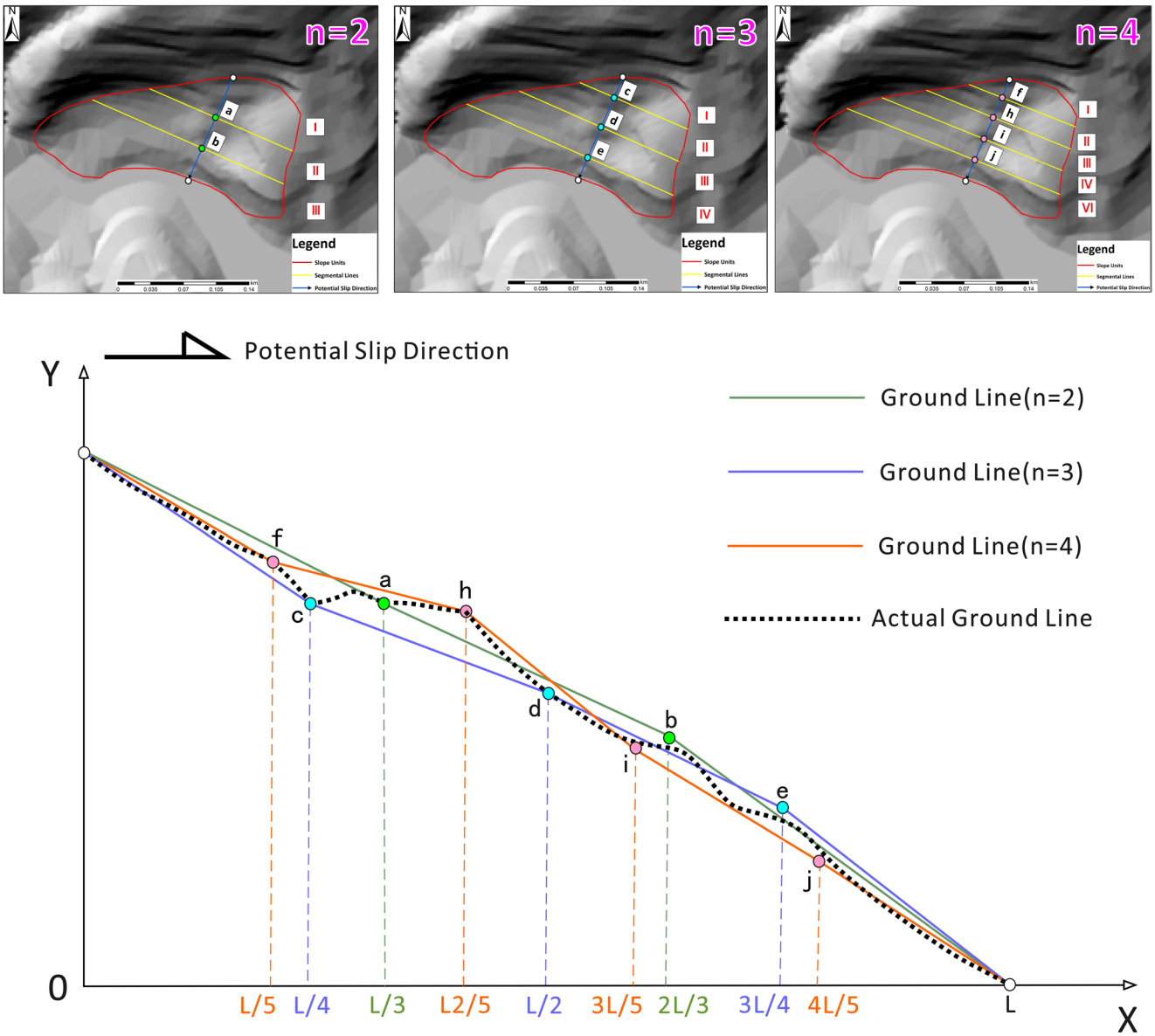

Fig. 5 Sketch map of segmental lines (n is the number of segmental lines)

Representative profile generation

Double lines representative profile

Double lines representative profile (Fig. 6) is made up of a ground line and a slip surface. Based on this type of profile, stability and failure probability can be calculated for each slope unit under natural conditions. As the regional landslide hazard susceptibility assessment is an analysis of the probability of occurrence for landslides under basic disaster-prone geological environmental conditions, it is not necessary to consider the influence of dynamic triggering factors, such as rainfall. Therefore, the failure probability calculated from the double line representative profile can be applied to the landslide susceptibility zoning.

The RPM uses the slope unit as the basic unit for the overall slope stability calculations. It assumes that the potential sliding surface intersects the slope at its leading and trailing edges, specifically at points P1 and P4. The ground line consists of the two endpoints of the potential slip direction line and the intersection of the mean slope line and the segment line, the vertical coordinates of each point being the corresponding DEM value.

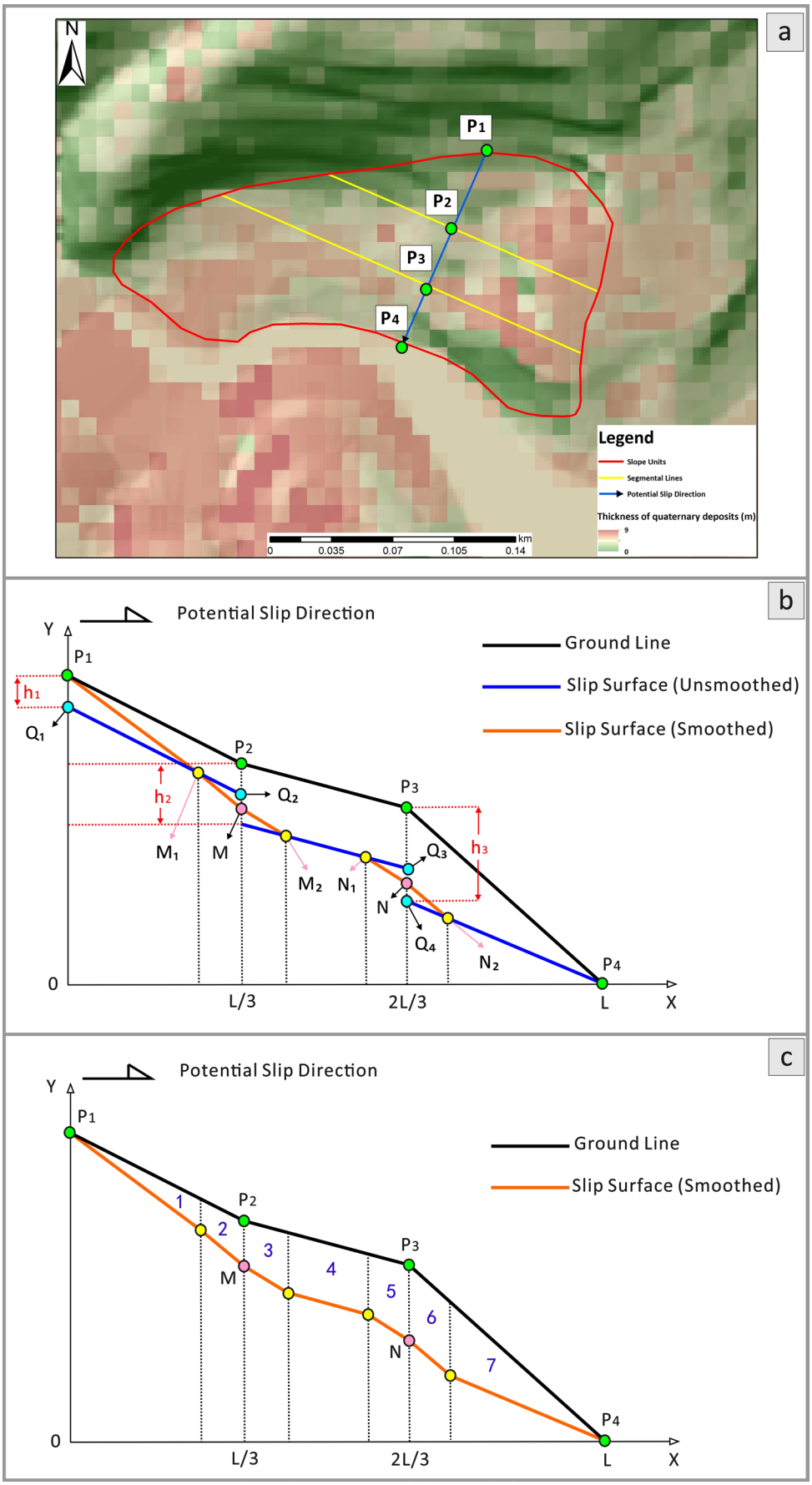

Fig. 6 Sketch map of double-line representative profile (**a**: slope-unit segmentation; **b**: initial slip surface—blue line shows ground line shifted downward by each segment's mean Quaternary-deposit thickness h_1, h_2, h_3—and smoothed slip surface shown by the orange line with transition points M and N; **c**: slice divisions, slices 1–7)

The initial slip surface was determined by translating each segment of the ground line downward by the average thickness of the Quaternary sediments in that segment. These segments are represented by the blue lines Q_1Q_2, Q_2Q_3, and Q_4P_4 in Fig. 6b. However, the segments of the initial slip surface did not connect seamlessly. To address this, the RPM introduced transition points (M and N in Fig. 6b) to smooth the surface. Transition point M is located at the midpoint of the line segment M_1M_2, where M1 is a point on Q_1Q_2, and the distance M_1Q_2 is 1/9 of Q_1Q_2. The other transition points are determined similarly. This empirically determined ratio provides a smooth transition and stable surface geometry without significantly altering the original slip surface shape. The other transition points are defined in the same manner.

Triple lines representative profile

For rainfall-induced landslides, the hydrological response is an important factor affecting landslide stability. In order to characterize the influence of hydrological factors on slope instability, RPM adds saturation lines to the double lines representative profiles to form triple lines representative profiles (Fig. 7). The shear strength parameters in the saturated state are used in the stability calculations for those parts of the slices located below the saturation line, while the shear strength parameters in the natural state are used for those parts of the slices located above the saturation line. Furthermore, in stability calculations, RPM considers the effect of hydrodynamic pressure. Following the determination of the factor of safety, the failure probability P_s for each slope unit under various rainfall conditions is solved using the Monte Carlo method as the basis for landslide hazard zoning.

The saturation line in the triple lines representative profile is generated using ground water level raster data obtained through TRIGRS, a USGS slope stability analysis program based on the infinite slope model. TRIGRS calculates the ground water level in the study area after a rainfall event based on input conditions such as initial ground water level, rainfall intensity, rainfall duration, and infiltration rate (Saadatkhah et al. 2016). The results of TRIGRS may have negative ground water levels, meaning that there is an overflow of ground water at the raster. If the average ground water level in a section of the slope unit is negative, our program sets the saturation line corresponding to that section of the cell to be consistent with the ground line. Additionally, in the triple lines representative profile, the saturation line is determined using the same method as for the slip surface (see subsection 2.3.1).

Slope failure probability analysis method

RPM employs the residual thrust method for assessing slope stability, incorporating dynamic water pressure to account for ground water effects within the traditional residual thrust equations (Ozbay et al., 2015; Huang et al. 2025) (Fig. 8). The residual thrust method is based on several simplifying assumptions, including a pre-defined slip surface, rigid body failure, homogeneity of soil properties along the slip surface, and two-dimensional analysis (Duncan et al., 2014; Abramson et al., 2001). Building upon the classical factor of safety analysis, RPM also integrates the Monte Carlo method to enhance the reliability of slope unit failure probability calculations.

The factor of safety F_s can be described by Eq. (1) :

$$F_s = \frac{\sum_{i=1}^{n-1}\left(R_i\prod_{j=1}^{n-1}\prod\psi_j\right)+R_n}{\sum_{i=1}^{n-1}\left(T_i\prod_{j=1}^{n-1}\psi_j\right)+T_n} \tag{1}$$

Where R_i is the anti-sliding force of the slice i, T_i is the slip force of slice i, and Ψ_j is the transfer coefficient when the residual sliding force of slice i is transferred to slice $i+1$ $(i=j)$. These two variables can be described by Eq. (2) ~ (4), respectively.

$$R_i = N_i tan\varphi_i + c_i l_i \tag{2}$$

$$T_i = W_i sin\theta_i + F_{sf}\cos\theta_i \tag{3}$$

$$\psi_j = cos\,(\theta_i - \theta_{i+1}) - sin\,(\theta_i - \theta_{i+1})\,tan\varphi_{i+1} \tag{4}$$

Where W_i is the weight of slice i, θ_i is the angle of inclination of the bottom of slice i, N_i is the component force of slice i in the normal direction of the slip surface, and F_{sf} is the hydrostatic pressure. These variables can be described by Eq. (5) to (8) respectively.

$$N_i = W_i cos\theta_i - F_{sf}\sin\alpha - F_{bf_i} \tag{5}$$

$$F_{sf} = \gamma_w sin\alpha \tag{6}$$

$$F_{bf_i} = \gamma_w V_{id} \tag{7}$$

$$W_i = \gamma V_{iu} + \gamma_{sat} V_{id} \tag{8}$$

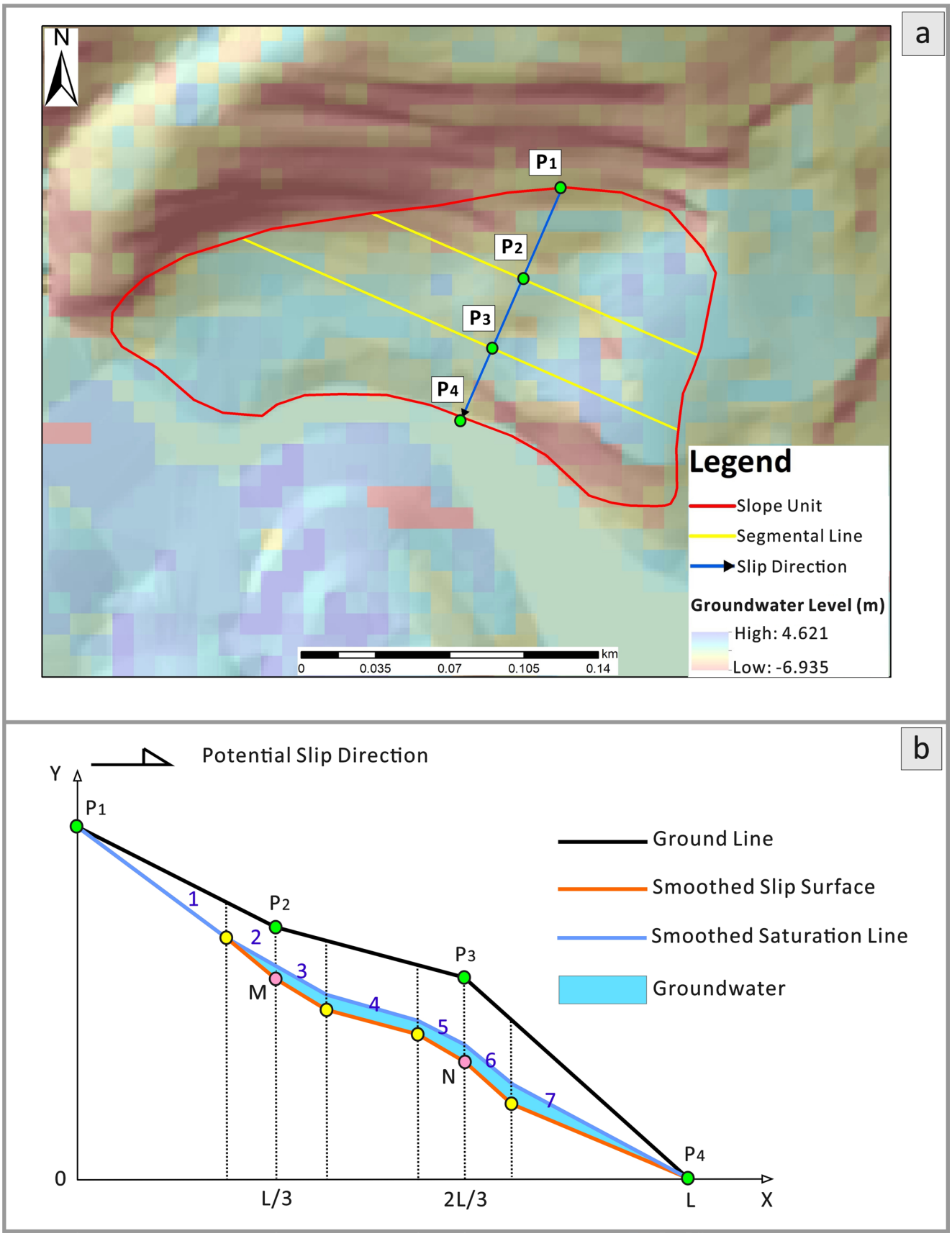
a
N
P1
P2
P3
P4
Legend
Slope Unit
Segmental Line
Slip Direction
Groundwater Level (m)
High: 4.621
Low: -6.935
km
0
0.035
0.07
0.105
0.14
b
Potential Slip Direction
Y
P1
P2
P3
P4
M
N
1
2
3
4
5
6
7
0
L/3
2L/3
L
X
Ground Line
Smoothed Slip Surface
Smoothed Saturation Line
Groundwater

Fig. 7 Sketch map of triple-line representative profile (**a**: the yellow line is the segmentation line dividing the slope unit into three segments, the blue line with black arrows represents the potential sliding direction; **b**: the black line represents the ground line, the blue line represents the smoothed infiltration line, the orange line represents the smoothed slip surface, the light blue shading represents groundwater)

Where c_i is the cohesion of the rock and soil body on the slip surface of slice i, φ_i is internal friction angle of slice i, l_i is the length of slice i, F_{bf_i} is the pore water pressure at the bottom of slice i, γ_w is the water weight, V_{iu} is the volume above the saturation line of slice i, V_{id} is the volume below the saturation line of slice i, γ is the natural weight of the geotechnical body, and γ_{sat} is saturated weight of the geotechnical body.

The Monte Carlo approach (Li et al. 2022), a statistical simulation method that repeatedly samples random variables to estimate the probability of a given outcome, is incorporated into the automatic analysis program developed for RPM. Users can specify the number of simulations N, and the program automatically assigns N random shear strength parameters following a normal distribution, then calculates N corresponding stability factors F_s using the residual thrust method. The number of cases where $F_s < 1$ is denoted as M, and the failure probability is estimated as Eq. 9.

$$P_s = \frac{M}{N} \tag{9}$$

Study area and data

Geologic setting and distribution of landslides

The study area is located in Tie Feng Township, north of Wan Zhou District, Chongqing, with longitude 108°20′34″ to 108°26′59″ east and latitude 30°55′31″ to 31°00′18″ north (Fig. 9). Tie Feng Township is 11.76 km long from east to west and 5.28 km wide from north to south, with a total area of 52.18km^2. The climate in the study area is subtropical monsoonal moderate and humid, with plenty of sunshine and rainfall. The area was selected as the study site mainly because of its high data availability and representativeness of rainfall-induced colluvial landslides in southwestern China. Specifically, Tie Feng Township provides well-documented geological, hydrological, and geomorphological datasets—including a detailed landslide inventory, over 1200 Quaternary deposit thickness measurements, and comprehensive rainfall records—which are essential for calibrating and validating the proposed physically based model.

The north-south profile of the study area forms a distinct "V" shape (Fig. 9b), with the central valley dividing it into an anaclinal slope on the north side and a cataclinal slope on the south. The Triassic (T), Jurassic (J), and Quaternary (Q) formations are exposed in Tie Feng Township, and their orientation is nearly east–west. The Triassic outcrops include the fourth section of the Badong Formation (T_2b_4), consisting chiefly of marl and shale, and the Xujiahe Formation (T_3xj), dominated by detrital quartz sandstone, silty mudstone, and shale. The Jurassic, from oldest to youngest, comprises the Pearl Chong Formation (J_1z), characterized by detrital quartz sandstone, mudstone, silty mudstone and shale; the Ziliujing Formation ($J_{1-2}z$), featuring quartz sandstone, bioclastic sandstone, rudaceous limestone and shale; the Xintiangou Formation (J_2x), made up of detrital quartz sandstone, shale and silty mudstone; and the Lower Shaximiao Formation (J_2xs), dominated by detrital quartz sandstone, mudstone and locally calcareous mudstone.

The study area lies on the northwestern flank near the hinge of the Tiefengshan anticline (Fig. 9c), which trends 50°~70° with its axis convex toward the NNW; the hinge zone is occupied by T_2b strata. Both flanks expose units from $J_{1-2}z$ to J_2xs: the northwestern flank dips 8°~30° (locally up to 47°), while the southeastern flank dips 45°~87°, with beds near the axis generally steep to overturned. Due to the differences in geological environment, the composition and thickness of the Quaternary deposits (Q) vary in the study area.

There are 23 colluvial landslides in the study area, as identified in the regularly updated landslide inventory collected from the local government. The landslides range in size from 984.97 m² to approximately 1.04×10^6 m². The landslide material mainly consists of colluvial deposits and landslide deposits. The sliding surface of colluvial landslides is at the boundary between bedrock and overlying Quaternary deposits. Some landslides have been investigated through drilling, with the sliding body thickness ranging from 2 m to 10 m, classified as medium-thickness and shallow landslides. The dip directions of the strata in the study area are approximately 330°. The southern slopes are mostly consequent slopes, while the northern slopes are predominantly reverse slopes. Therefore, the majority of the landslides in the study region are on the south side of the study area, in the consequent slope area (18 landslides). Only a few smaller landslides are found on the north side of the study area's reverse slope (5 landslides). The slopes of the colluvial landslides in the area generally range from 10° to 20°, with varying degrees of topographical undulation. Topography is the main factor controlling landslide boundaries. The lateral boundaries

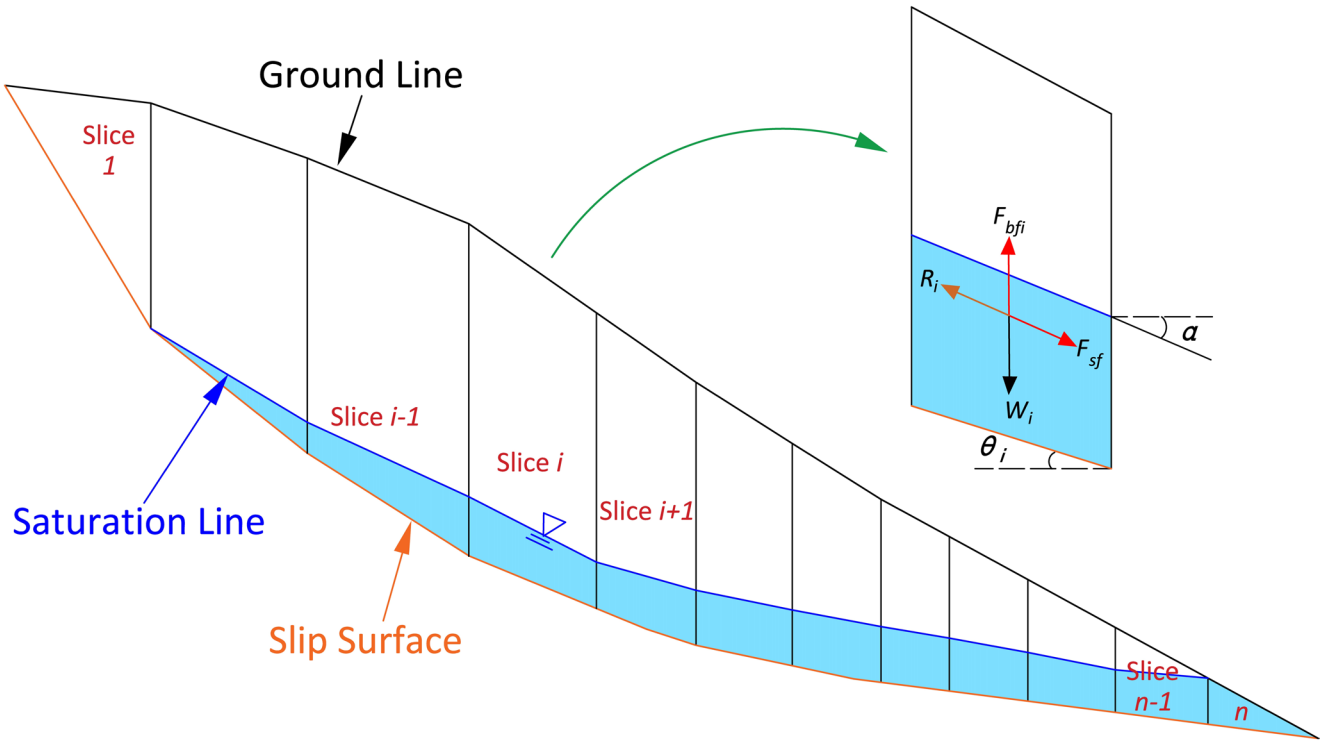

Fig. 8 Mechanical calculation model of safety factor

of landslides often develop along valleys. Rainfall is the primary trigger for landslides in the study area, with most landslides experiencing instability or rapid deformation during heavy rainfall periods. Some landslides are influenced by road cutting.

In addition to colluvial slides, the study area experienced a major translational rockslide on 5 September 2004 (Fig. 9a). While an exceptionally intense rainfall event (200 mm/day) provided the initial trigger, the primary driver was toe cutting during road-construction excavation at the slope's front edge. This failure was further aggravated by the underlying dip-slope structure and the presence of soft, interbedded rock layers on the southern flank. The resultant debris has since remained a readily mobilizable source for downstream soil-slide activity. In the aftermath, local authorities recognized that unregulated, large-scale engineering works significantly heightened landslide risk. They therefore implemented stringent management measures, and, owing to these controls, no similar incidents have been recorded in the years that followed. Moreover, Du et al. (2025) demonstrate that the construction of rural roads in Tiefeng Township has led to the formation of numerous steep rock slopes; the excavation process fractures the rock masses on these slopes, generating large volumes of unstable rock and triggering rockfalls. As for debris flows, or earth flows, none have been recorded in the local government's disaster inventory. Overall, rainfall-induced colluvial landslides remain the dominant hazard type in the study area. Accordingly, the RPM model was specifically developed and calibrated to simulate this type of failure. The choice of this study area is therefore appropriate for evaluating the performance and applicability of RPM.

Slope units

Since grid cells do not account for the entirety of a landslide, the RPM uses slope units as the fundamental units of analysis. Slope units are considered to be watersheds delineated by ridge lines and valley lines (Xie et al. 2014; Zeng et al., 2024; Xiao et al., 2020; Zhang et al., 2024). In this study, a total of 1237 slope units were generated using hydrological analysis methods (Alvioli et al. 2020; Yan et al. 2017; Huo et al., 2011) within the ArcGIS environment (Fig. 10). The average size of the slope units was 0.0334 km², with the vast majority being smaller than 0.05 km². Among the 23 landslides identified, the smallest area was 9.85×10^{-4} km², the largest was 1.04 km², and the average area was 0.03 km². Thus, the slope units generated in this study are dimensionally consistent with the landslides.

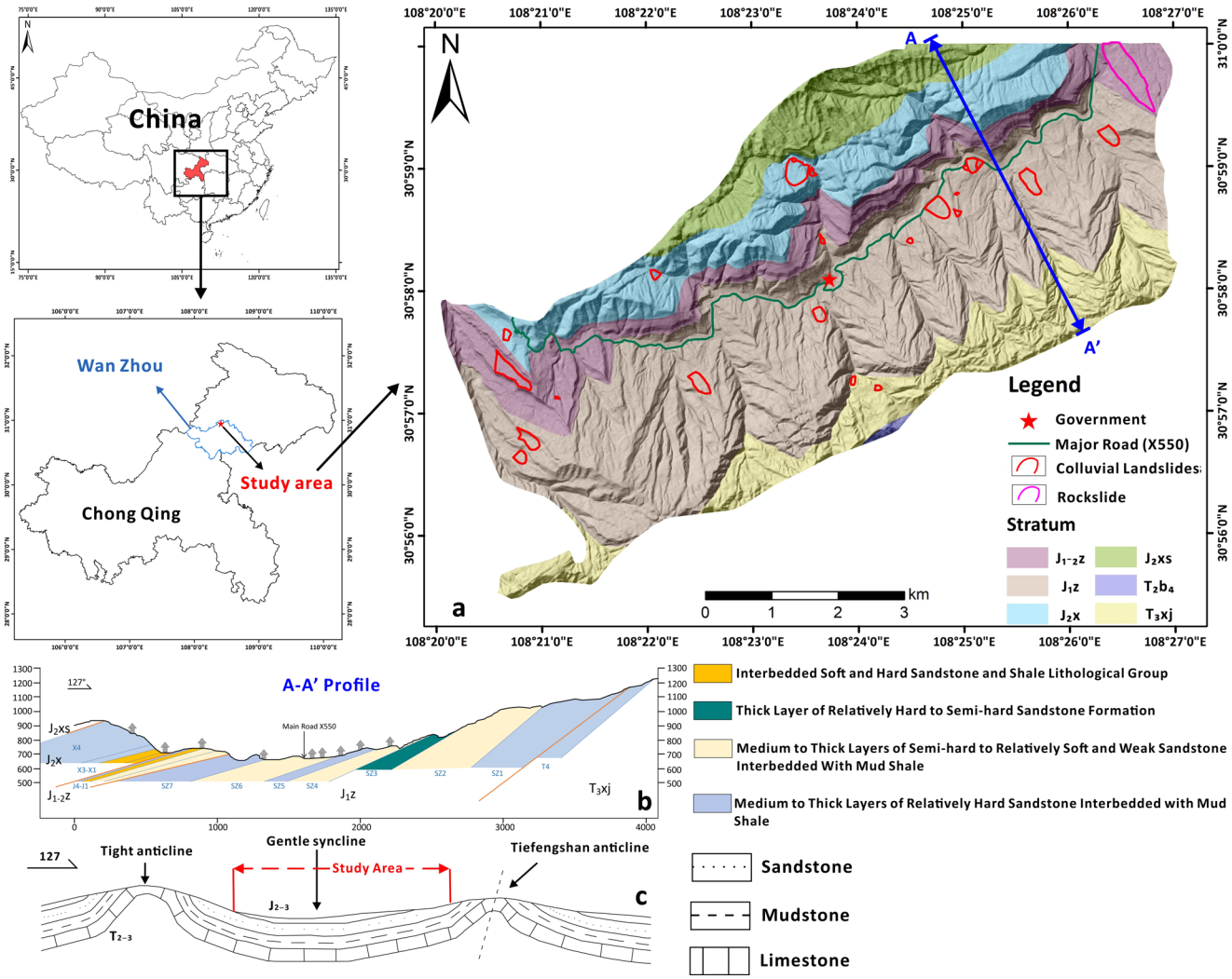

Fig. 9 The study area and distribution of landslides (**a**: Distribution of landslides and geological formations in the study area; **b**: A–A' profile showing the lithological units within different strata of the study area; **c**: Geological structures of the study area)

Field investigation of quaternary deposits

The Quaternary deposits in the studied area are very well developed, however, the types and thickness of the deposits vary greatly in terms of spatial distribution. Quaternary deposits are extensively developed in the study area, but their types and thicknesses vary greatly across the region. The Quaternary deposits are mainly classified into two categories: residual deposits, and landslide and collapse deposits. Residual deposits are continuously distributed along the crest and upper to middle portions of the dip slopes on the southern side of the study area. Due to well-developed surface vegetation in these areas, surface runoff has limited erosive and transport capacity, so the thickness of residual deposits is closely related to the underlying bedrock lithology. Softer rocks (such as siltstone interbedded with mudstone, or shale) tend to produce thicker residual deposits, while harder rocks (such as quartz sandstone) are associated with thinner residual layers. Residual deposits are generally dense, fine-grained, and have a high soil-to-rock ratio (Fig. 11b). Collapse deposits are mainly distributed on the western side of the study area, where the alternation of soft and hard strata, together with favorable lateral free-face conditions, promotes their formation. Collapse deposits are characterized by loose structure, a high proportion of rock fragments, and significant heterogeneity (Fig. 11a). Overall, due to lithological differences, areas underlain by softer rocks are characterized by gentler slopes and thicker collapse deposits, whereas areas with harder rocks have steeper slopes and thinner collapse deposits.

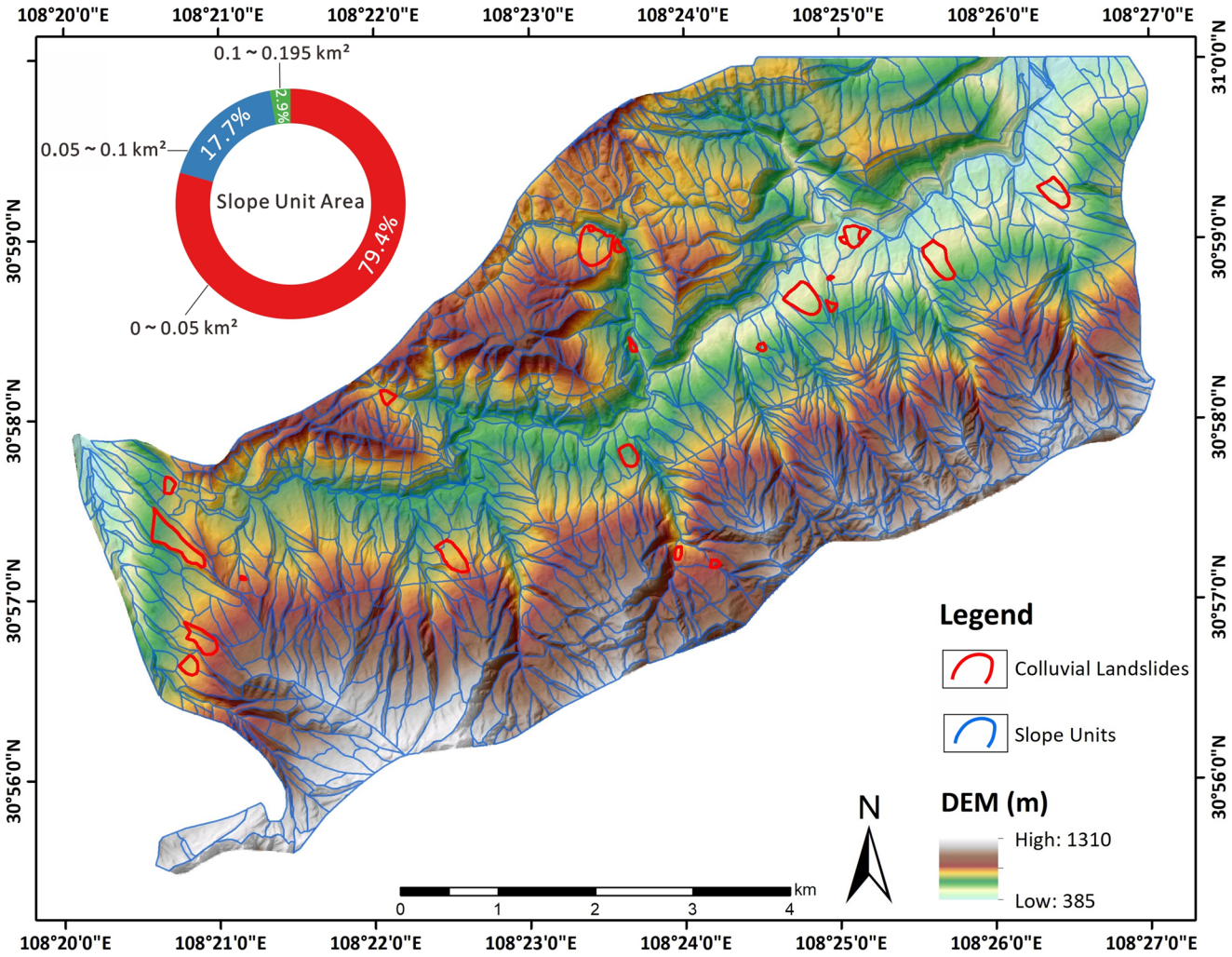

Fig. 10 Slope units of study area

To study the spatial distribution of Quaternary deposits thickness in Tie Feng Township, 1211 Quaternary deposits thickness sample points were collected in the study area during the field investigation (Fig. 11). Considering the objective differences in shear strength parameters for different types of Quaternary deposits, we have taken the values of shear strength parameters for different types of deposits based on previous survey data (Wang et al. 2020a, b; Xiao et al. 2020) in the area as shown in Table 1.

Results

Quaternary deposits thickness

In the RPM, the accuracy of the Quaternary deposits thickness data will directly affect the reasonableness of the slices in the calculated profile of each slope unit, which in turn affects the accuracy of the final stability calculation results. Therefore, this paper proposes a coupled data mining and machine learning approach to obtain the accurate spatial distribution of the thickness of the Quaternary deposits in the study area.

Firstly, 13 factors that may affect the distribution of the thickness of the Quaternary deposits were proposed, and then the correlation was analyzed using the Maximal Information Coefficient (MIC), which measures both linear and nonlinear relationships between variables, with higher MIC values indicating stronger associations. The calculation results are shown in Table 2. The MIC of six factors, including slope, aspect, flow direction, topographic relief, profile curvature, and slope structure, are of the same order of magnitude, and their correlation with the thickness of Quaternary deposits is more significant than the other seven factors, Therefore, they are selected as the indicators for predicting the thickness of Quaternary deposits.

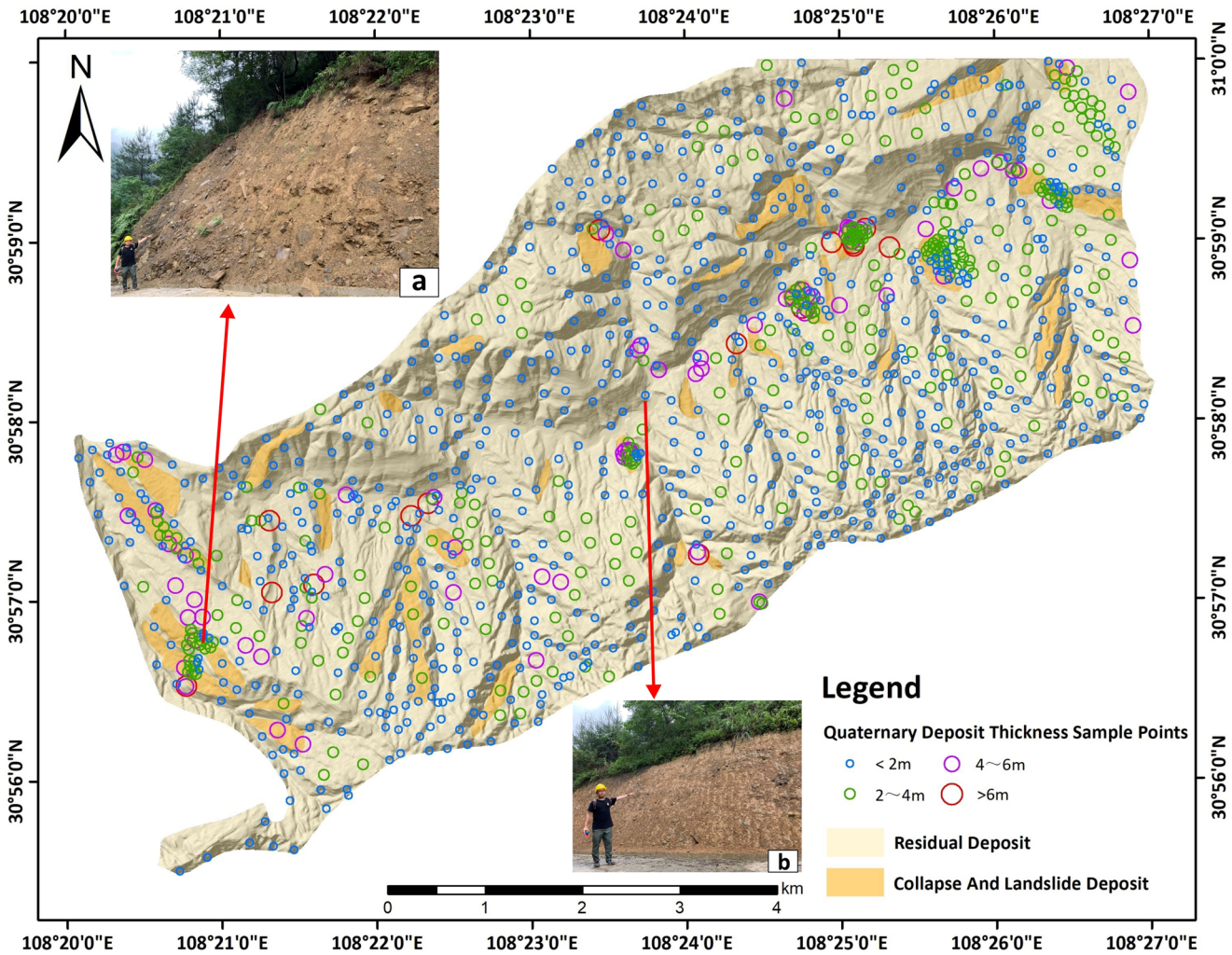

Fig. 11 Field survey points for Quaternary deposits (**a**: a field survey point of collapse deposits with a thickness of approximately 4 m; **b**: a field survey point of landslide deposits with a thickness of approximately 1.9 m)

Table 1 Shear strength parameters of different types of quaternary deposits

Type of Quaternary deposits	c(kPa)		φ (°)		γ (kN/m^3)	
	Natural Mean/Variance	Saturated Mean/Variance	Natural Mean/Variance	Saturated Mean/Variance	Natural Mean/Variance	Saturated Mean/Variance
Residual deposits	10.9/2.8	8.7/2.4	12.1/3.4	9.3/2.7	21.6/4.3	22.4/4.2
Collapse and landslide deposits	9.1/2.7	7.4/2.2	10.4/4.1	8.1/3.2	15.3/4.1	17.6/4.1

80% of the 1,211 thickness sample points in the study area were used as the training set, and the remaining 20% as the test set. This sampling ratio has been widely adopted in previous studies (Yang et al. 2023; Tang et al. 2023; Huang et al. 2024). Six machine learning models were employed to predict the thickness of the Quaternary deposits (Table 3), each combining an optimization algorithm with a basic predictive model to improve performance. Specifically, Particle Swarm Optimization (PSO; Marini et al., 2015), Genetic Algorithm (GA; Lambora et al. 2019), and Grey Wolf Optimization (GWO; Mirjalili et al. 2014) were used as optimization algorithms, while Support Vector Machine (SVM; Pisner et al., 2020), Extreme Learning Machine (ELM; Wang et al. 2022), Back Propagation Neural Network (BPNN; Suliman et al., 2015), and Least Squares SVM (LSSVM; Leong et al. 2021) served as the base models. The six combinations (PSO–SVM, PSO–ELM, PSO–BPNN, PSO–LSSVM, GA–SVM, and GWO–SVM) were trained using six selected indicators as input variables and the measured Quaternary deposit thickness as the target variable. Model performance was then evaluated on the test set to identify the one with the highest prediction accuracy.

As shown in Table 3; Fig. 12, the predicted values of each model in the test set fit the true values well overall,

Table 2 Results of factor correlation degree mining

Factors	MIC
Slope	**0.6977**
Aspect	**0.5285**
Flow Direction	**0.4696**
Elevation	0.0752
Water Catchment	0.0417
Topographic Relief	**0.6933**
Stratum	0.0486
Distance From Water System	0.0525
Distance From Cliff	0.0637
Profile Curvature	0.2141
Plane Curvature	0.0784
Structure of Slope	**0.3271**
NDVI	0.0943

Table 3 Error indexes of each model

Model	MSE	RMSE	Q	C
PSO—SVM	401.22	1.42	0.47	0.79
PSO—ELM	202.24	1.01	0.28	0.78
PSO—BPNN	689.08	1.86	0.81	0.83
PSO—LSSVM	705.32	1.88	0.83	**0.71**
GA—SVM	198.57	1.00	0.23	0.76
GWO—SVM	**152.24**	**0.87**	**0.19**	0.83

but some models occasionally had large deviations. Model performance was evaluated using four commonly used statistical indicators: mean squared error (MSE) and root mean squared error (RMSE), which measure the average and root-average magnitude of prediction errors; Q, which reflects the model bias; and C, which represents the correlation between predicted and observed values. GWO-SVM outperforms the others in the test set, with MSE of only 152.24, RMSE of only 0.87, and Q of only 0.19, and the best overall accuracy. The GWO-SVM model was used to carry out the prediction of the thickness of the Quaternary deposits in the study area, and the results are shown in Fig. 12.

From the predicted results (Fig. 13), the thickness of Quaternary deposits is thinnest at the cliffs of the reverse slopes in the northern part of the study area. Similarly, thin accumulations are observed on both sides of the deeply incised gullies in the southern part. The eastern and western sides of the study area, characterized by dip slopes, exhibit substantial thicknesses ranging from 3 to 9 m. This may be attributed to the slope structure and the combination of alternating soft and hard stratigraphic lithologies, which are prone to landslide disasters. Historically, this area has experienced landslide events, leading to the formation of thick landslide deposits. For example, a large bedding plane landslide (Minguochang landslide) was induced by heavy rainfall on the eastern side of the study area. Additionally, on the reverse slopes in the northern part of the study area, thicker Quaternary materials have accumulated at the foot platforms of cliffs due to the deposition of landslide materials. The slope materials on the northern and southern sides mainly comprise residual slope deposits, with a thickness of approximately 1–3 m.

Ground water level

The spatial distribution of groundwater levels is a key input parameter for the RPM. In this study, we employed TRIGRS model, which has been widely used to simulate rainfall-induced changes in subsurface hydrology at the slope scale and provides reliable estimates of groundwater level distribution for landslide hazard assessment. TRIGRS simulates the dynamic response of pore water pressures and groundwater levels to rainfall infiltration by solving the one-dimensional vertical flow equation, making it particularly suitable for capturing the transient hydrological processes that control shallow landslide initiation (Iverson et al., 2000). Its ability to account for both saturated and unsaturated flow allows for realistic

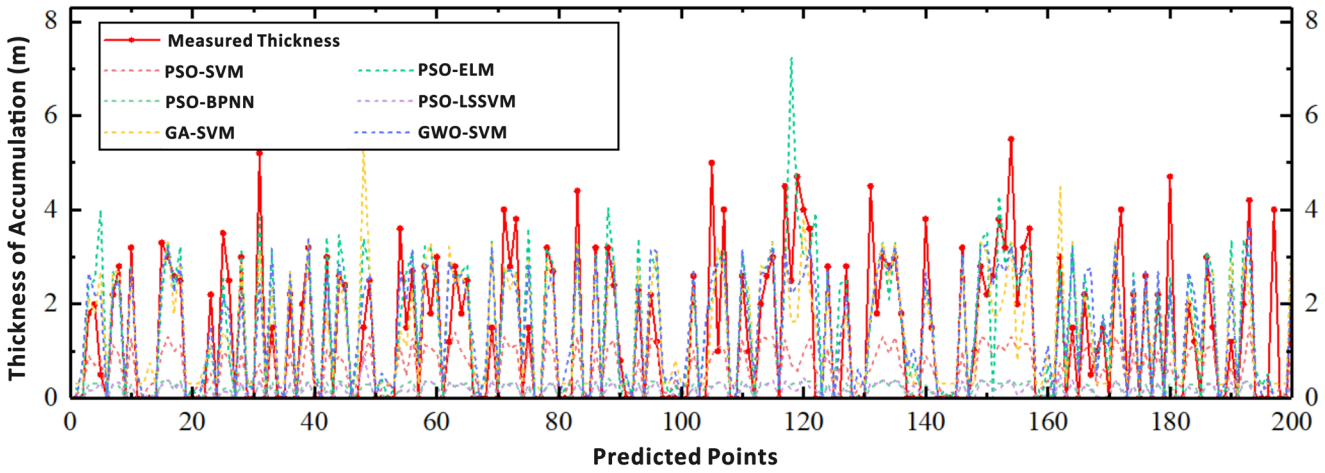

Fig. 12 Accuracy of each model

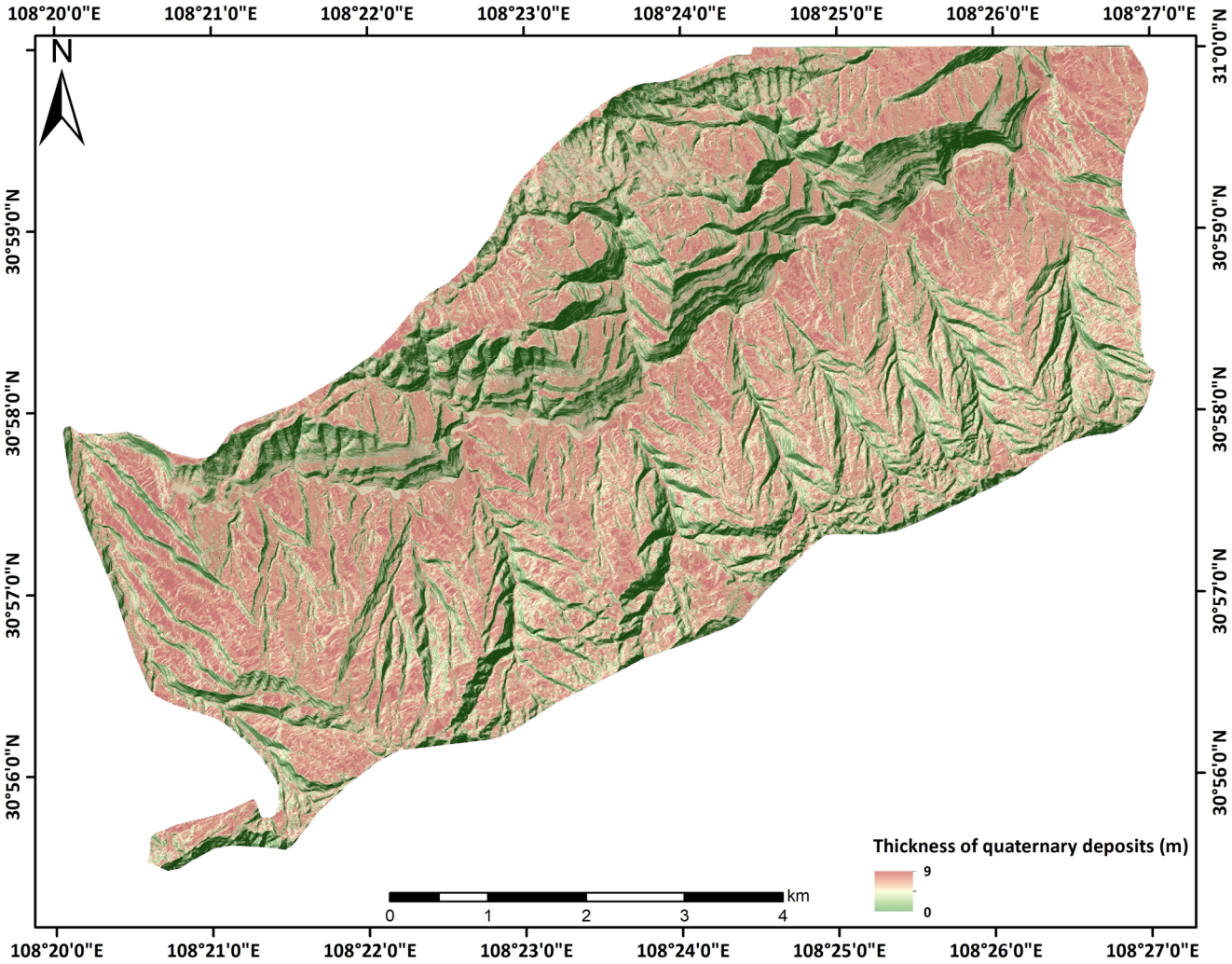

Fig. 13 Prediction of quaternary deposits thickness

Table 4 Simulation parameters (h is the thickness of quaternary deposits)

Working condition	initial water level(m)	infiltration rate(m/s)	rainfall intensity(m/s)	time(s)
Weak rainfall	1.5 h	10^{-7}	3.86×10^{-7}	172,800
Storm rainfall	1.5 h	10^{-7}	1.16×10^{-6}	259,200

prediction of groundwater table fluctuations under different rainfall scenarios. Using TRIGRS, we simulated groundwater level distributions across the study area under both intense storm and mild rainfall conditions. The initial settings used in the TRIGRS simulations (Tran et al. 2017; Salciarini et al. 2008; Baum et al., 2010) are detailed in Table 4, and the resulting groundwater level distributions are presented in Fig. 14.

The results of the ground water level simulations for the two rainfall conditions were shown in Fig. 14. Ground water level in the study area gradually rises with increasing rainfall intensity and rainfall duration. During the storm rainfall conditions, the ground water level in the whole area of Tie Feng Township was generally high, with the shallowest part being only about 0.5 m from the surface and the infiltration line being closer to the slope surface. Ground water overflow occurs locally due to the relatively thin Quaternary deposits.

Landslide susceptibility assessment

A total of 1237 slope units were divided in the study area, and the double lines representative profile of each slope unit was generated using the self-developed RPM integration assessment program. The failure probability calculated based on the double lines representative profile was used as the grading standard for assessing the susceptibility of colluvial landslide in the study area.

The results of susceptibility zoning are shown in Fig. 15. Of the 1237 units, 1 (0.08%) unit belong to the very high susceptibility zone, 39 (3.15%) units belong to

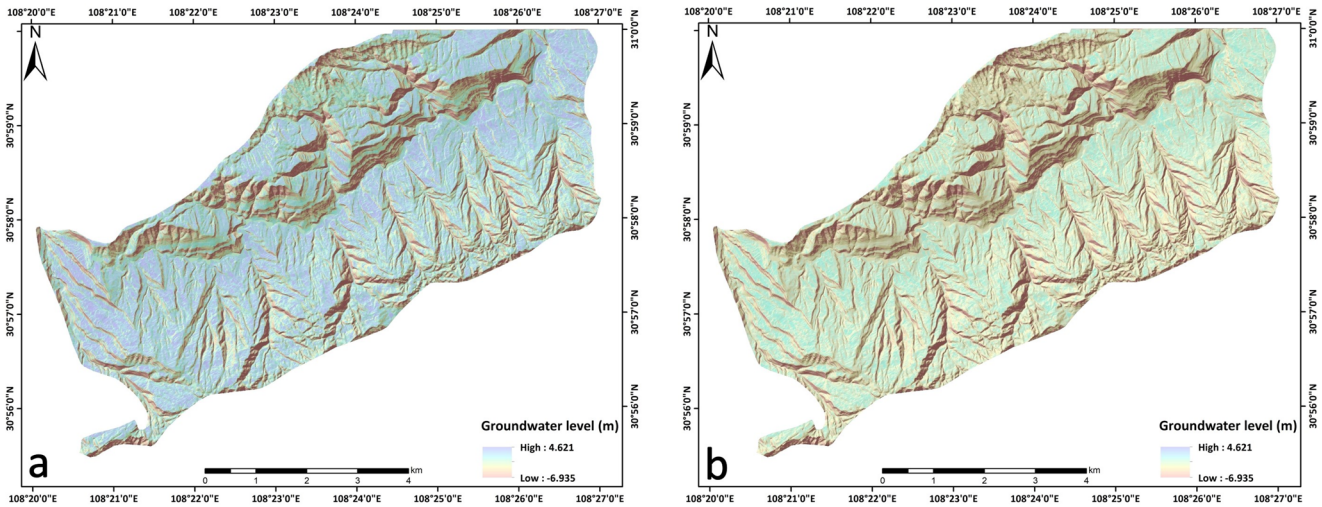

Fig. 14 Simulation results of ground water level (**a**. weak rainfall condition; **b**. storm rainfall condition. Positive values indicate the distance between the ground water level and the slope surface. Negative values signify that ground water has formed slope runoff at that location.)

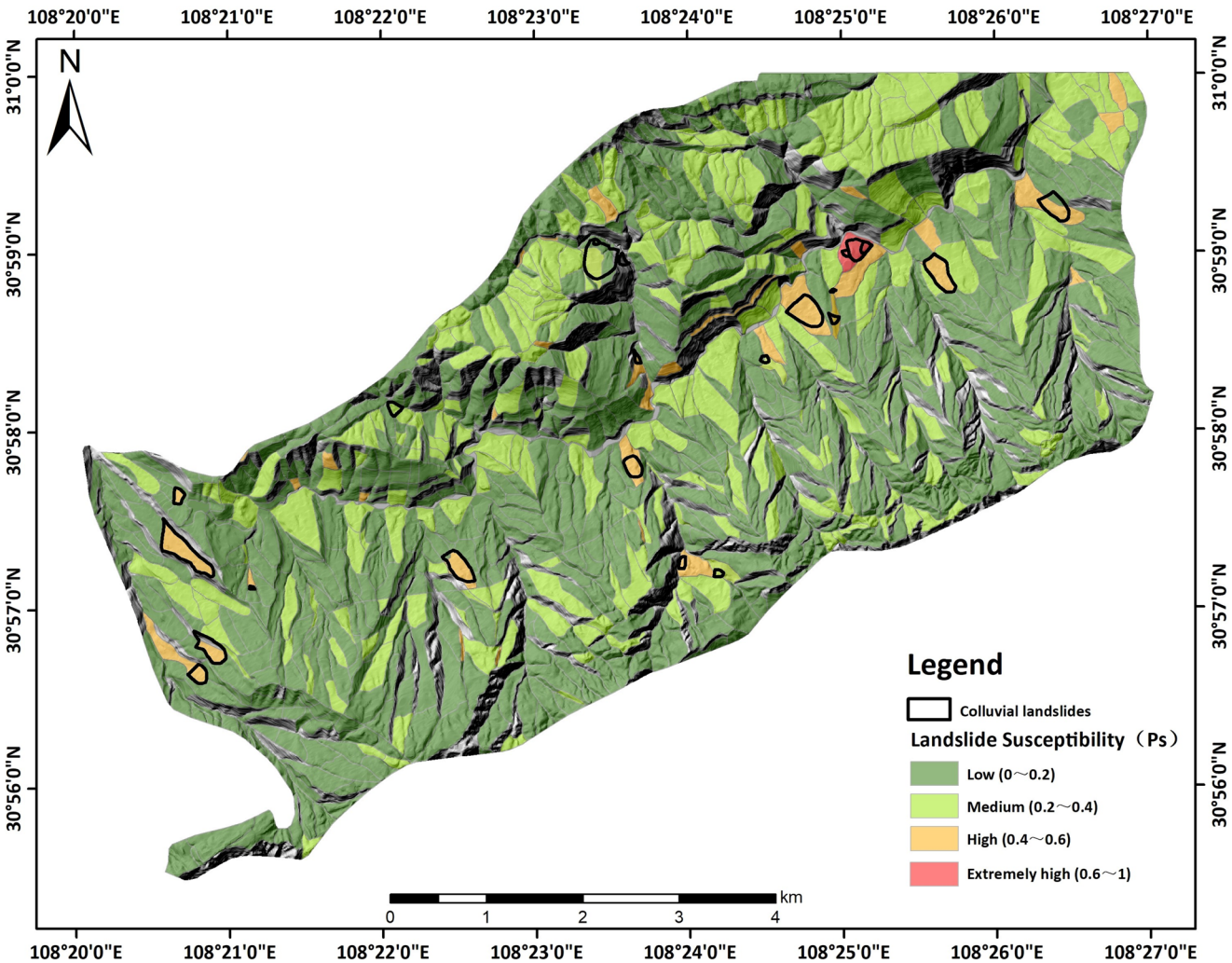

Fig. 15 Zoning map of colluvial landslide susceptibility in Tie Feng Township

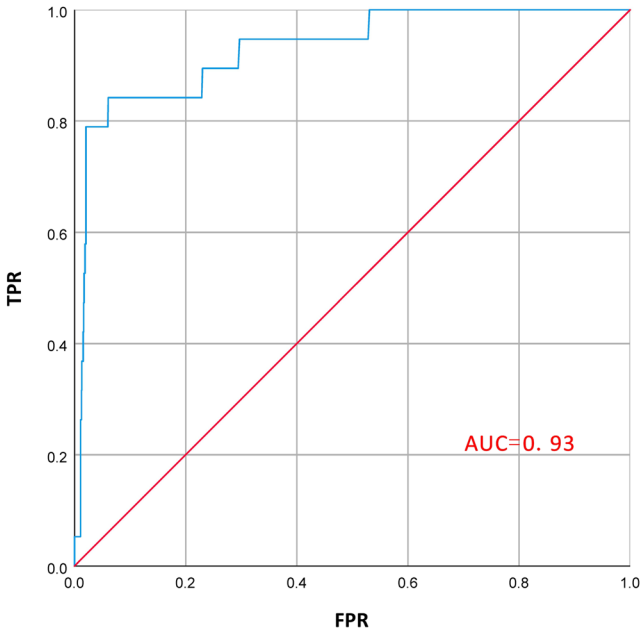

Fig. 16 The ROC curve

the high susceptibility zone, 279 (22.55%) units belong to the medium susceptibility zone, and 918 (74.22%) units belong to the low susceptibility zone. On the whole, the slope units in the central part of Tie Feng Township near County Road X550 and the northeastern part of the township are more prone to colluvial landslides, because the slope units in this area are mostly cataclinal slope structures with thick overlying Quaternary deposits, which provide good material conditions for colluvial landslides to occur. Of the 22 historical colluvial landslides, 3 landslides (13.64%) are in very high susceptibility areas, 15 landslides (68.18%) are in high susceptibility areas, 3 landslides (13.64%) are in medium susceptibility areas and 1 landslide (4.54%) are in low susceptibility areas. The overall accuracy of the assessment results is relatively high and in line with the actual situation.

In order to quantitatively assess the accuracy of the calculation results, ROC curves were plotted for the failure probability P_s of 1237 slope units, where the state variable was set to 1 for units where landslides occurred and 0 for units where no landslides occurred. The ROC curve provides a graphical representation of the model's ability to distinguish between positive and negative cases, while the area under the curve (AUC) quantifies its overall discriminative power, with values closer to 1 indicating better performance. As shown in Fig. 16, the AUC value of the failure probability P_s reached 0.93, indicating that the results of the susceptibility assessment are consistent with the actual situation, and RPM's performance for susceptibility assessment was relatively good.

Landslide hazard assessment

In this section, the self-developed integrated assessment software for RPM is used to generate the triple lines representative profile for each slope unit, and the failure probability calculated based on the triple lines representative profile is used as the grading criterion for evaluating the hazard of colluvial landslide in the study area. The results of the landslide hazard assessment under weak rainfall conditions are shown in Fig. 17. Overall, most of Tiefeng Township under weak rainfall conditions is dominated by low to moderate landslide hazard, with a small number of high-risk units occurring in the centre of township, and only one slope unit assessed as being at very high risk, with three historical landslides distributed within this unit. The number of medium hazrad units in Tiefeng Township under weak rainfall conditions has increased more significantly compared to the results of the susceptibility assessment that did not take into account the effects of rainfall and ground water.

Figure 18 shows the results of RPM calculations under storm rainfall conditions. The number of medium hazard units increased compared to the weak rainfall conditions. There are 63 high-hazard units in study area, mainly concentrated along County Road X550, showing a continuous distribution. There are 13 very high-hazard units, mainly located along the downward slope on the east side of County Road X550. However, there are also individual units in the north and south anaclinal slope sections of the study area that are high and extremely high hazards. The majority of the historical colluvial landslides are in high and extremely high-hazard units, with a few in medium to low-hazard units. It is necessary to maintain a focus on the areas where the extremely high-hazard units are located during storm rainfall in the flood season and to have some geohazard managers stationed nearby to assist in evacuating residents in the event of a dangerous situation.

Discussion

Comparison with TRIGRS

To further illustrate the advantages of RPM for assessing hazard of colluvial landslides at a regional scale, we used the widely used TRIGRS to calculate the landslide hazard of the study area (the calculation parameters are shown in Table 1), and the results were compared with those of RPM.

Figure 19 illustrates the differences in the results of the two models under heavy rainfall conditions. As rainfall increases, both TRIGRS and RPM calculations show

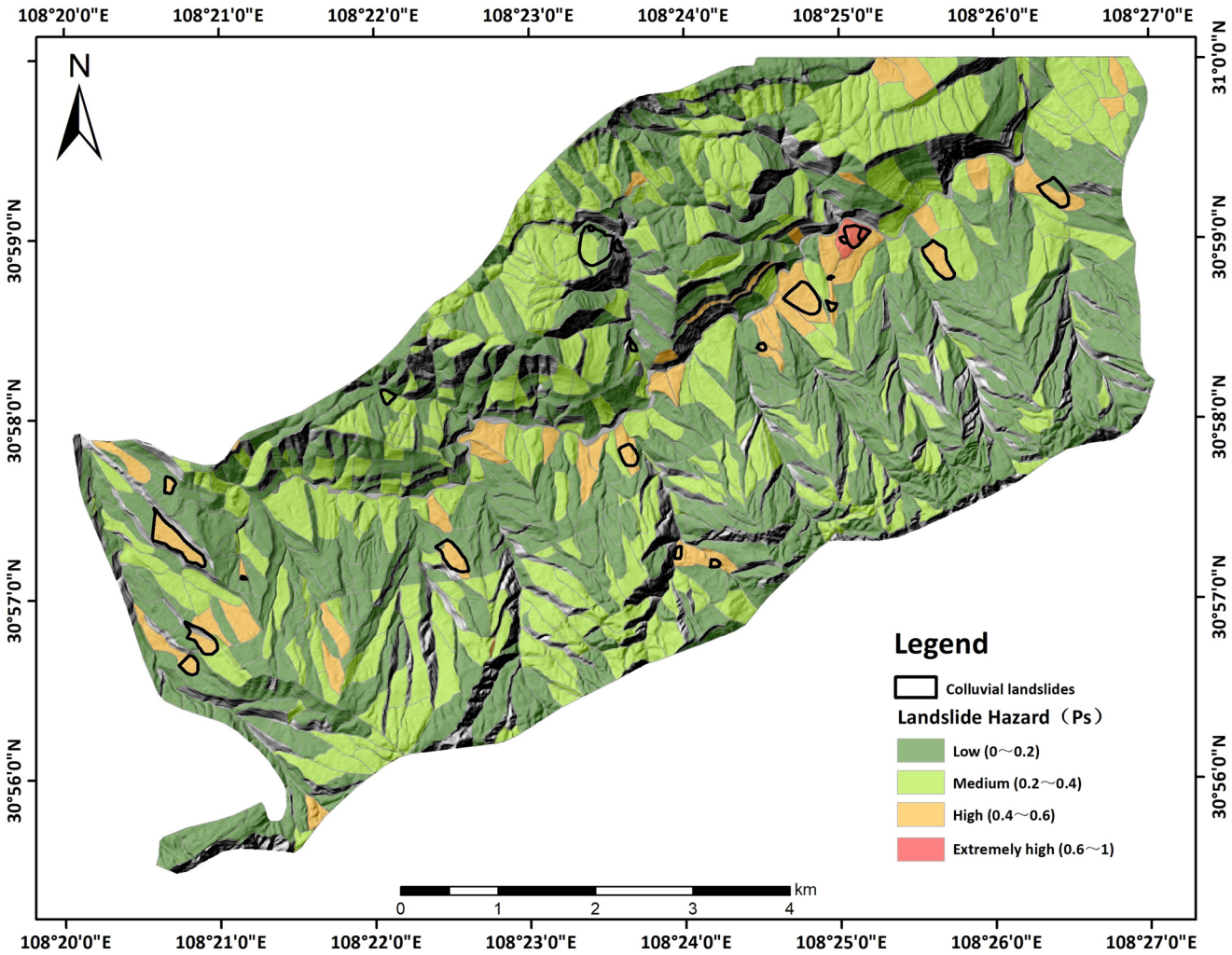

Fig. 17 Hazard zoning of colluvial landslides under weak rainfall conditions

a significant increase in the overall instability of the study area, and the area near the middle of the study area is assessed as a high hazard area in both models' calculations, indicating that the landslide hazard assessment capabilities of TRIGRS and RPM are similar over a larger area. However, the stability calculation accuracy of the TRIGRS model is still unsatisfactory in local areas. Our field investigation of a slope unit with sliding roadbeds, cracked house walls and small roadside collapses within the unit (Fig. 19d, e) indicates that the slope unit is currently in a less stable state, but the TRIGRS calculations show that the unit is in a largely stable state, which is clearly unreasonable. As a comparison, the representative model assesses this slope unit as very high risk, which is more in line with the results of the field survey.

This case study demonstrates that the RPM model has superior landslide hazard assessment capabilities compared to the TRIGRS model on a regional scale. The primary reason is that RPM uses slope units in calculating stability, whereas TRIGRS uses raster units and assumes a parallel relationship between the sliding surface and the ground surface. Numerous previous studies have proven that slope units better characterize the structure of landslide topography than raster units for landslide disasters (Burton et al. 1998; Li & Lan, 2020; Wang et al. 2025; Liu et al., 2025).

Raster units discretely partition the complete slope unit, with each evaluation unit representing the stability of an independent raster, unable to reflect the true structure of the entire slope (such as the slope face gradient variations, the potential sliding surface morphology, and the interactions between different parts of the slope). Consequently, TRIGRS results in high-hazard evaluation units concentrated in steeper areas, failing to accurately depict the overall stability of slope units prone to landslides.

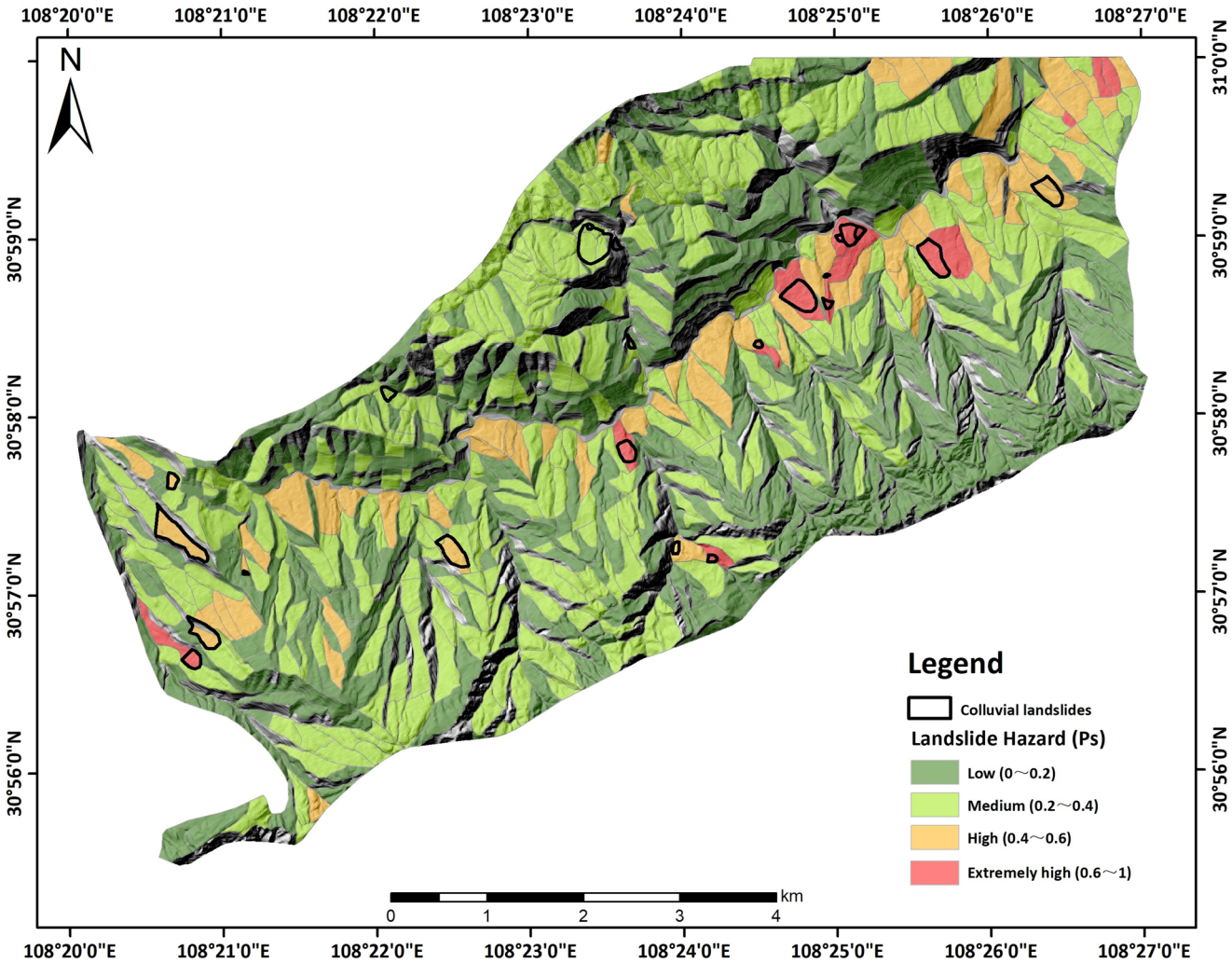

Fig. 18 Hazard zoning of colluvial landslides under storm rainfall condition

For example, in Fig. 19, the thickness of Quaternary deposits at points a and b are notably thin, and the overall profile exhibits a pattern of a steep rear and a gentle front. This configuration is generally unfavorable for landslide formation. Stability calculations for the representative profile indicate that it has not reached a high hazard status. However, TRIGRS identified this location as a high hazard area because it only assesses the stability of each raster individually. Nevertheless, field investigations revealed that the slope at this location showed no signs of landslide deformation. Furthermore, with regard to point d and e, the raster units around point d are less stable due to the steeper gradient, while the raster units around point e are more stable due to the gentler gradient. Such a spatial distribution of raster stability makes it difficult to recognize the overall poor stability of the slope. In contrast, the RPM method uses complete, independent slope units for evaluation. By extracting segments, it presents the overall two-dimensional structural characteristics of the landslide through representative profiles. For example, in the slopes shown in Fig. 18, points d and e, the lower part of the slope has a steeper gradient while the upper part is gentler. Considering the sliding surface depth and groundwater level changes, the overall stability of the slope is calculated to be low, thus providing direct scientific guidance for regional geological disaster risk management. Therefore, compared with the infinite slope theory, RPM is more suitable for landslide susceptibility and hazard assessment at a regional scale.

Sensitivity analysis of key parameters in RPM

RPM utilizes three-dimensional real surface data, deposit depth, and groundwater level data, segmenting slopes according to elevation. Within each segment, it uses the average values of these factors to achieve a more accurate

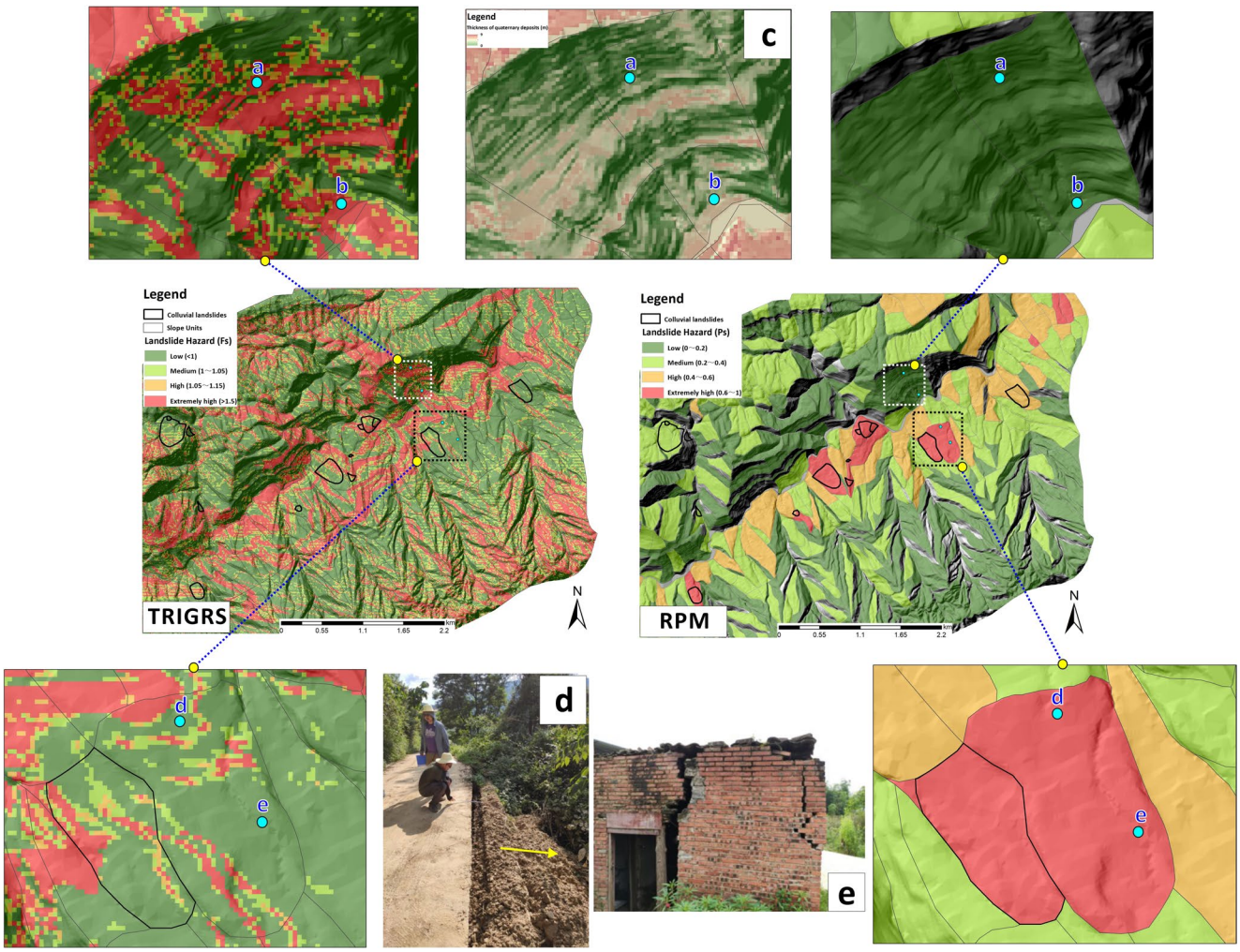

Fig. 19 The comparison between RPM and TRIGRS (under storm rainfall conditions)

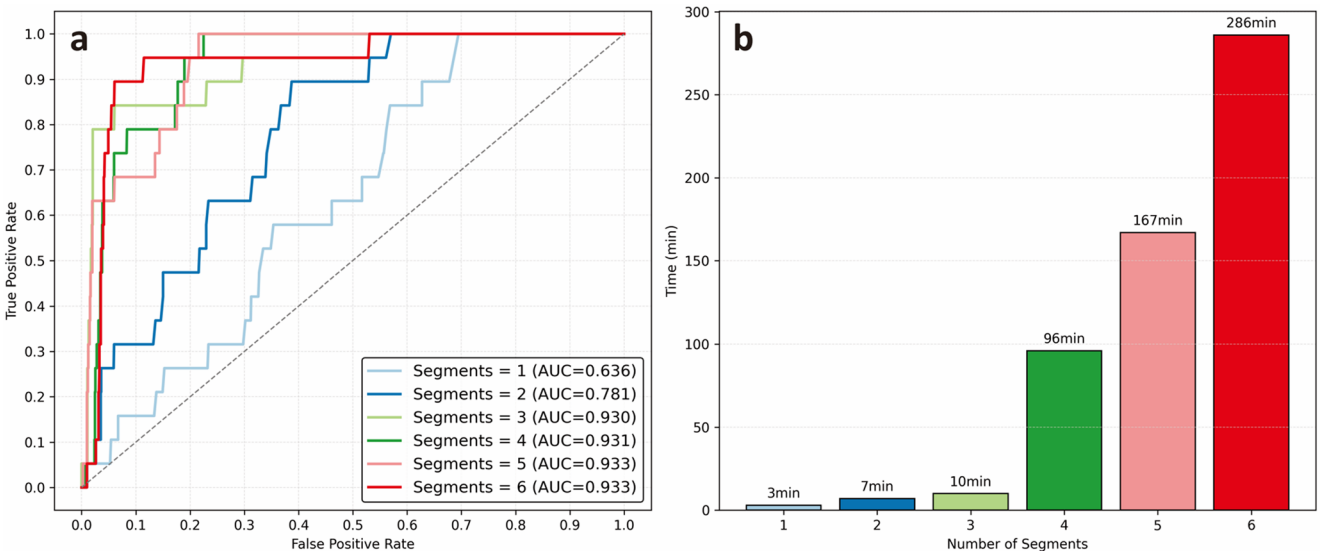

Fig. 20 Impact of segment count on RPM performance and runtime (**a**, ROC curves and AUC values for RPM models with 1–6 segments; **b**, bar chart of computation time in minutes for each segment count)

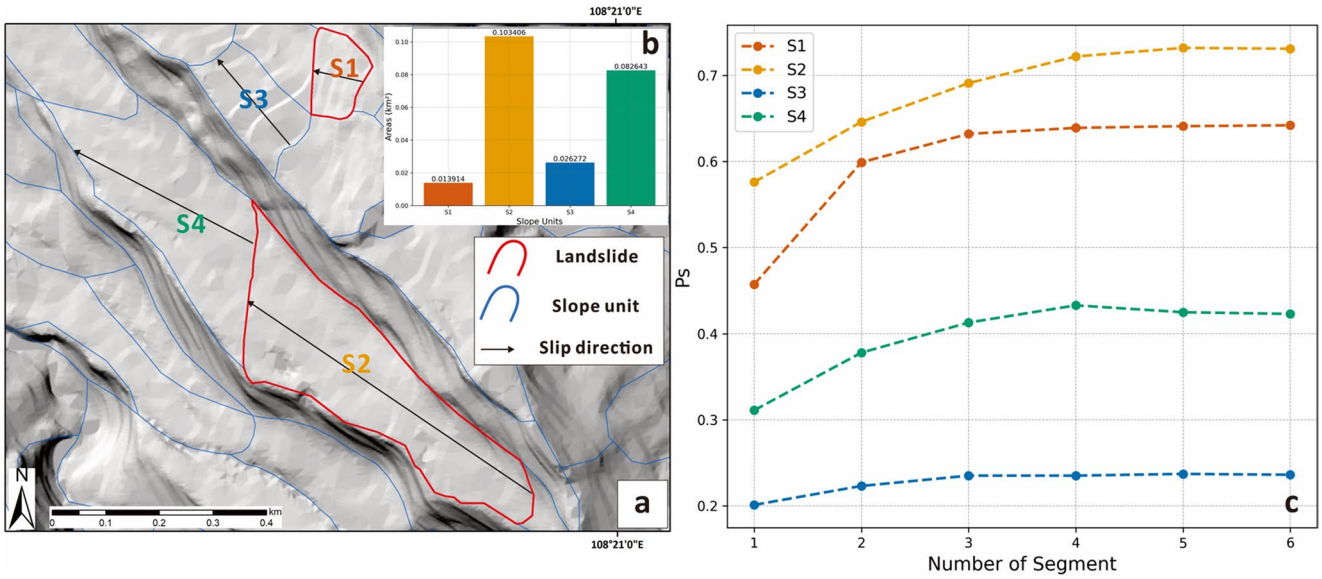

Fig. 21 Sensitivity of slope units of different sizes to the number of segments (**a**, slope units S1 and S2 that have experienced historical landslides versus the non-failed units S3 and S4; **b**, bar chart of the areas of the four slope units; **c**, trends of RPM-calculated failure probability Ps for each slope unit as the segment-line count increases)

two-dimensional representation of the slope's three-dimensional characteristics. In this process, the determination of the number of segments involves a degree of subjectivity and relies on experiential judgment. Since the number of segments is a critical factor in RPM, directly affecting the accuracy of the terrain profiles generated for each slope unit, this subsection specifically discusses the optimal setting of the number of segments.

Theoretically, increasing the number of segments results in terrain profiles that more closely approximate the actual slope, thereby yielding a more precise estimation of slope failure probabilities. However, the benefits associated with increasing the number of segments are not unlimited. To illustrate this point, we evaluated the RPM's predictive performance (expressed as the AUC value) and computational cost using a double-segment profile configuration by varying the number of segments from 1 to 6 (Fig. 20). The results indicate that increasing the segments from 1 to 3 substantially improved the RPM's AUC from 0.636 to 0.930, while the corresponding computational time remained acceptable (within 10 min). However, further increasing the segments to 4, 5, and 6 resulted in negligible improvements in the AUC (a maximum increase of only 0.003), whereas computational time rose sharply to 286 min—approximately 28 times longer than with 3 segments. Therefore, for the study area examined here, three segments represent the optimal setting, achieving high predictive accuracy (AUC = 0.930) with minimal computational cost (10 min).

Furthermore, the sensitivity of slope units of different sizes to the number of segments also varies. To investigate this variability, we selected two smaller-scale slope units (S1 = 0.013914 km^2, S3 = 0.026272 km^2) and two larger-scale slope units (S2 = 0.103406 km^2, S4 = 0.082643 km^2) for further sensitivity analysis (Fig. 21a, b). Among these units, two had previously experienced landslides (S1, S2), while the other two had not (S3, S4). The results indicate that for smaller-scale slope units, the failure probability calculated by RPM generally does not change once the number of segments reaches three. In contrast, larger-scale slope units require additional segments before their failure probability converges (Fig. 21c). Therefore, when implementing RPM in practice, careful consideration should be given to the scale of the slope units. For larger slope units, it may be necessary to set a higher number of segmentation lines to achieve the most accurate calculation of failure probability.

Assumptions adopted by RPM

Landslide instability and failure is a non-linear process impacted by a variety of elements such as rainfall, snowmelt, and earthquakes (González et al. 2017; Oliveira et al. 2016; Lashgari et al. 2025; Oliveira et al., 2024). However, since it is not possible to account for all of the influencing factors when constructing the computational equations for a physically-based model, appropriate simplification of the influencing factors is necessary (Sun et al. 2016). Like other landslide models based on the physical process, RPM has also been simplified to some extent: (i) RPM averages the geological parameters in each segment; (ii) The sliding mass slides downward along the average slope direction. Furthermore, no

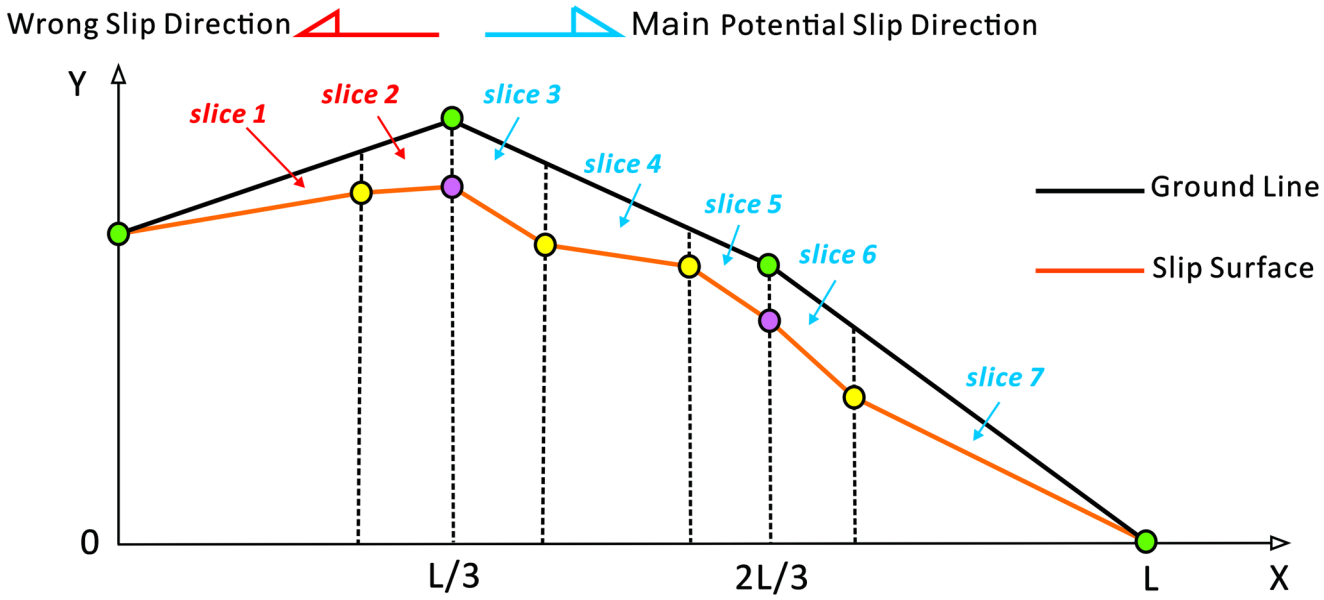

Fig. 22 Schematic diagram of an improperly delineated slope unit (The initial slices 1 and 2 are counter-dip slices, whose potential sliding directions are opposite to the overall orientation of the slope unit)

single physically-based model can be applied to all types of landslide stability assessment, and the same is true for RPM, it is only applicable to the assessment of the stability of earthy landslides that slide along the base cover interface. A potential future enhancement of the RPM would be to incorporate the effects of seismic loading or to integrate the Newmark method (Montoya et al., 2025); Peláez et al. 2025) into the stability calculation. This would enable the RPM to be used for assessing the stability of earthquake-induced landslides.

Impact of slope unit quality

In addition, as the slope unit is the basic unit for RPM's landslide susceptibility and hazard assessment, the quality of the slope unit will have a direct impact on the RPM's assessment outcomes. The slope units in this study were delineated by extracting primary ridge-valley lines through hydrological analysis, followed by manual adjustments based on microtopography features. However, some issues remain with the delineation of certain units, resulting in a "rising then falling" pattern in the corresponding two-dimensional representative profiles. This causes the initial slices to slide in the opposite direction to the potential sliding direction of the slope (Fig. 22), leading these initial slices to provide "resisting forces" against sliding, which is clearly not reasonable. To address this, the RPM code for calculating safety factors has been optimized so that these initial inverse slices are ignored in the calculation.

Currently, several scholars have proposed automated methods for slope unit delineation (Alvioli et al.2016 ; Wang et al. 2019; Huang et al. 2021; Li et al. 2024; Woodard et al. 2024), which are capable of producing higher-quality slope units. Therefore, integrating these slope unit generation algorithms into the automated workflow of RPM would be a highly promising improvement, potentially enhancing both the applicability and accuracy of the model.

Regional-scale geotechnical parameters

As one of the physically-based models, RPM also has the common limitation of the others, i.e., it is difficult to obtain the precise shear strength parameters, especially at a regional scale (Cai et al. 2017; Ip et al. 2021; Mathews et al. 2024; Dahal et al., 2025). Limited by the lack of shear strength parameters in the study area, this study cannot obtain the spatial distribution law of mechanical parameters, so we can only give empirical values for each slope unit according to their type of overlying quaternary deposits. However, since the RPM incorporates the Monte Carlo method, the geotechnical parameters of each slope unit are not identical—even for units with the same type of deposits. This approach greatly minimizes the impact of parameter uncertainty at the regional scale.

More accurate geotechnical parameters would, of course, significantly improve the performance of the RPM as well as all other physically-based models. Several possible approaches for improvement include: (i) utilizing widely distributed InSAR data and back-analysis models to invert geotechnical parameters at the regional scale (Medwedeff et al. 2025; Bunn et al. 2020); (ii) constructing large

geotechnical engineering datasets based on extensive in-situ sample testing, and employing data mining techniques to identify and predict the spatial distribution patterns of geotechnical parameters at the regional scale; and (iii) developing data-driven predictive methods that can account for the spatial heterogeneity of geotechnical parameters.

The ease of use and transferability of RPM

RPM is well robust for tasks such as stability calculations of slope units at a regional scale and evaluation of colluvial landslide susceptibility and hazard. In order to improve the transferability of the RPM, we have developed a software package with a graphical interactive interface based on the C#.NET language for the entire calculation process, which allows users to quickly apply RPM to the assessment of colluvial landslide susceptibility and hazard in other areas. Unlike console programs based on Fortran language such as TRIGRS, RPM has a UI interface, which saves a lot of tedious.txt format-based file calculation settings and data conversion. The input and output of data are more intuitive, which reduces the user's learning cost and is conducive to rapid promotion.

Conclusions

In this study, a new physically-based model, the RPM, was proposed, which was applied to assess landslide susceptibility and hazard in Tiefeng Town, Wanzhou District, Chongqing Municipality, China. Compared with the traditional raster-based infinite slope model, the RPM model significantly improved the accuracy of large-scale regional susceptibility and hazard assessment of colluvial landslides. The main contributions of this paper are as follows:

4. A physically-based, slope unit-based regional landslide hazard assessment model—RPM—was developed, and an automated calculation program for RPM was implemented in C#. Unlike the traditional raster-based infinite slope model, RPM uses slope units as the basic calculation unit, which allows consideration of topographic variability and interactions between different parts of a slope. RPM requires a digital elevation model (DEM) and Quaternary deposit thickness data to generate a representative double line profile for each slope unit, which is then used to calculate the failure probability for susceptibility assessment. In addition, for hazard assessment, RPM integrates groundwater level data to generate representative triple line profiles.
5. Regional-scale Quaternary deposit thickness was predicted using machine learning methods. A dataset was constructed based on 1,211 field measurements of Quaternary deposit thickness, with 80% of the data randomly assigned for training and 20% for testing. Six machine learning models were established (PSO-SVM, PSO-ELM, PSO-BPNN, PSO-LSSVM, GA-SVM, and GWO-SVR). Error analysis indicated that the GWO-SVR model performed best (MSE = 152.4, RMSE = 0.87), and this model was used to generate a high-resolution Quaternary deposit thickness map for the study area—one of the key input datasets for RPM.
6. A case study was conducted in Tiefeng Township, Wanzhou District, Chongqing, demonstrating the effectiveness of RPM and its advantages over the widely used infinite slope model, TRIGRS. The TRIGRS model was used to estimate groundwater levels under both mild and intense rainfall scenarios. The RPM model was then employed for landslide susceptibility and hazard assessment. The results showed that the RPM method achieved an area under the ROC curve (AUC) of 0.93, with 75% of historical landslides occurring in units classified as highly or extremely susceptible, indicating that RPM provides an effective approach for regional landslide susceptibility assessment. Furthermore, field investigations revealed that RPM-based hazard assessment results were more accurate, whereas the TRIGRS model exhibited significant overestimation and underestimation.

Although RPM has some limitations, such as the use of simplified computational formulas, reliance on the quality of slope units for accurate assessment results, and the challenge of obtaining high-precision geotechnical parameters on a regional scale, it offers significant advantages over traditional raster-based infinite slope models. By performing stability calculations based on slope units and accounting for the influence of topographic relief and interactions between different parts of a complete slope, RPM aligns more closely with the future trend of deterministic models for regional-scale slope stability assessment.

Acknowledgements This research was supported by the National Natural Science Foundation of China [Grant No. 42172318, 42377186, 42077277]. The authors thank the colleagues in our laboratory for their constructive comments and assistance. Furthermore, we would like to express our special gratitude to Professor Thom Bogaard from Delft University of Technology for his review and revision of the language of this paper.

Declarations

Competing interest None.

References

Abramson LW, Lee TS, Sharma S, Boyce GM (2001) Slope stability and stabilization methods. Wiley

Achu AL, Aju CD, Di Napoli M, Prakash P, Gopinath G, Shaji E, Chandra V (2023) Machine-learning based landslide susceptibility modelling with emphasis on uncertainty analysis. Geosci Front 14(6):101657

Agboola G, Beni LH, Elbayoumi T, Thompson G (2024) Optimizing landslide susceptibility mapping using machine learning and geospatial techniques. Ecol Informatics 81:102583

Al-Najjar HA, Pradhan B (2021) Spatial landslide susceptibility assessment using machine learning techniques assisted by additional data created with generative adversarial networks. Geosci Front 12(2):625–637

Alvioli M, Baum RL (2016) Parallelization of the TRIGRS model for rainfall-induced landslides using the message passing interface. Environ Model Softw 81:122–135

Alvioli M, Marchesini I, Reichenbach P, Rossi M, Ardizzone F, Fiorucci F, Guzzetti F (2016) Automatic delineation of geomorphological slope units with r. slopeunits v1. 0 and their optimization for landslide susceptibility modeling. Geosci Model Dev 9(11):3975–3991

Alvioli M, Guzzetti F, Marchesini I (2020) Parameter-free delineation of slope units and terrain subdivision of Italy. Geomorphology 358:107124

Brilli N, Masi EB, Rossi G, Tofani V (2025) Slope stability modelling of shallow landslides at a regional scale. Geoenviron Disasters 12(1):18

Baum, R. L., Godt, J. W., & Savage, W. Z. (2010). Estimating the timing and location of shallow rainfall-induced landslides using a model for transient, unsaturated infiltration. Journal of Geophysical Research: Earth Surface, 115(F3).

Bunn M, Leshchinsky B, Olsen MJ (2020) Geologic trends in shear strength properties inferred through three-dimensional back analysis of landslide inventories. J Geophys Res Earth Surf 125(9):e2019JF005461

Burton A, Arkell TJ, Bathurst JC (1998) Field variability of landslide model parameters. Environ Geol 35:100–114

Cai JS, Yeh TCJ, Yan EC, Hao YH, Huang SY, Wen JC (2017) Uncertainty of rainfall-induced landslides considering spatial variability of parameters. Comput Geotech 87:149–162

Caleca F, Lombardo L, Steger S, Tanyas H, Raspini F, Dahal A, Tofani V (2025) Pan-European landslide risk assessment: from theory to practice. Rev Geophys 63(1):e2023RG000825

Chang Z, Catani F, Huang F, Liu G, Meena SR, Huang J, Zhou C (2023) Landslide susceptibility prediction using slope unit-based machine learning models considering the heterogeneity of conditioning factors. J Rock Mech Geotech Eng 15(5):1127–1143

Chen X, Chen W (2021) Gis-based landslide susceptibility assessment using optimized hybrid machine learning methods. CATENA 196:104833

Cui H, Medina V, Hürlimann M, Ji J (2024a) Fast physically-based probabilistic modelling of rainfall-induced shallow landslide susceptibility at the regional scale considering geotechnical uncertainties and different hydrological conditions. Comput Geotech 172:106400

Cui H, Ji J, Hürlimann M, Medina V (2024b) Probabilistic and physically-based modelling of rainfall-induced landslide susceptibility using integrated GIS-FORM algorithm. Landslides 21(6):1461–1481

Dahal A, Lombardo L (2025) Towards physics-informed neural networks for landslide prediction. Eng Geol 344:107852

de Oliveira NS, Filho R, Marton OC, E., Silva C (2016) Correlation between rainfall and landslides in Nova Friburgo, Rio de Janeiro—Brazil: a case study. Environ Earth Sci 75:1–12

Dehnavi A, Aghdam IN, Pradhan B, Varzandeh MHM (2015) A new hybrid model using step-wise weight assessment ratio analysis (SWARA) technique and adaptive neuro-fuzzy inference system (ANFIS) for regional landslide hazard assessment in Iran. CATENA 135:122–148

Du J, Feng X, Chai B, Yin K, Zheng L (2025) Physically based deterministic rockfall hazard assessment integrating multi-failure modes at large scale: a case study of Tiefeng Township, Chongqing, China. J Rock Mech Geotech Eng. https://doi.org/10.1016/j.jrmge.2024.12.023

Duncan JM, Wright SG, Brandon TL (2014) Soil strength and slope stability. Wiley

Durmaz M, Hürlimann M, Huvaj N, Medina V (2023) Comparison of different hydrological and stability assumptions for physically-based modeling of shallow landslides. Eng Geol 323:107237

Eu S, Seo J, Lee K, Woo C, Lee C (2025) Nonstructural landslide mitigation of the Republic of Korea. Landslides 22(3):763–772

Feng X, Du J, Wu M, Chai B, Miao F, Wang Y (2024) Potential of synthetic images in landslide segmentation in data-poor scenario: a framework combining GAN and transformer models. Landslides 21(9):2211–2226

Froude MJ, Petley DN (2018) Global fatal landslide occurrence from 2004 to 2016. Nat Hazards Earth Syst Sci 18(8):2161–2181

Goetz JN, Brenning A, Petschko H, Leopold P (2015) Evaluating machine learning and statistical prediction techniques for landslide susceptibility modeling. Comput Geosci 81:1–11

González AAM, Passini LB, Kormann ACM (2017) Rainfall effects on pore pressure changes in a coastal slope of the Serra do Mar in Santa Catarina. Soils Rocks 40(3):263–278

Guo Z, Torra O, Hürlimann M, Abancó C, Medina V (2022) FSLAM: a QGIS plugin for fast regional susceptibility assessment of rainfall-induced landslides. Environ Model Softw 150:105354

Guzzetti F, Cardinali M, Reichenbach P, Carrara A (2000) Comparing landslide maps: a case study in the Upper Tiber River Basin, Central Italy. Environ Manage. https://doi.org/10.1007/s002679910020

Guzzetti F, Mondini AC, Cardinali M, Fiorucci F, Santangelo M, Chang KT (2012) Landslide inventory maps: new tools for an old problem. Earth Sci Rev 112(1–2):42–66

He J, Qiu H, Qu F, Hu S, Yang D, Shen Y, Cao M (2021) Prediction of spatiotemporal stability and rainfall threshold of shallow landslides using the TRIGRS and Scoops3D models. CATENA 197:104999

Huang F, Tao S, Chang Z, Huang J, Fan X, Jiang SH, Li W (2021) Efficient and automatic extraction of slope units based on multi-scale segmentation method for landslide assessments. Landslides 18:3715–3731

Huang F, Xiong H, Jiang SH, Yao C, Fan X, Catani F, Chang Zhilu, Zhou Xiaoting, Huang Jinsong, Liu K (2024) Modelling landslide susceptibility prediction: a review and construction of semi-supervised imbalanced theory. Earth Sci Rev 250:104700

Huang X, Wang G, Zhang L (2025) An analytical solution for critical sliding surface of stepped rock slope: a case study of Xinjing coal mine landslide. Bull Eng Geol Environ 84(2):78

Huo A, Zhang J, Lu Y, Cheng YC, Yao YL (2011) Method of classification for susceptibility evaluation unit for geological hazards: a case study of Huang Ling County. Shaanxi China J Jilin Univ (Earth Sci Ed) 41:523–528

Ip SC, Satyanaga A, Rahardjo H (2021) Spatial variation of shear strength properties incorporating auxiliary variables. Catena 200:105196

Iverson RM (2000) Landslide triggering by rain infiltration. Water Resour Res 36(7):1897–1910

Ji J, Tong B, Cui HZ, Tang XT, Hürlimann M, Du S (2025) A QGIS framework for physically-based probabilistic modelling of landslide susceptibility: QGIS-FORM. Environ Model Softw 183:106258

Kim H, Lee JH, Park HJ, Heo JH (2021) Assessment of temporal probability for rainfall-induced landslides based on nonstationary extreme value analysis. Eng Geol 294:106372

Lambora A, Gupta K, Chopra K (2019), February Genetic algorithm-A literature review. In 2019 international conference on machine learning, big data, cloud and parallel computing (COMITCon) (pp. 380–384). IEEE

Lashgari A, Rahimi L, Ahmadisharaf E, Barari A (2025) Probabilistic pre-conditioned compound landslide hazard assessment framework: integrating seismic and precipitation data and applications. Landslides 22(2):413–434

Leong WC, Bahadori A, Zhang J, Ahmad Z (2021) Prediction of water quality index (WQI) using support vector machine (SVM) and least square-support vector machine (LS-SVM). Int J River Basin Manage 19(2):149–156

Li L, Lan H (2020) Integration of spatial probability and size in slope-unit-based landslide susceptibility assessment: a case study. Int J Environ Res Public Health 17(21):8055

Li C, Wang G, He J, Wang Y (2022) A novel approach to probabilistic seismic landslide hazard mapping using Monte Carlo simulations. Eng Geol 301:106616

Li Y, Fu B, Han Z, Fang Z, Chen N, Hu G, Chen G (2024) Pso-slic algorithm: a novel automated method for the generation of high-homogeneity slope units using DEM data. Geomorphology 463:109367

Lin W, Yin K, Wang N, Xu Y, Guo Z, Li Y (2021) Landslide hazard assessment of rainfall-induced landslide based on the CF-SINMAP model: a case study from Wuling mountain in Hunan Province, China. Nat Hazards 106:679–700

Liu Z, Gilbert G, Cepeda JM, Lysdahl AOK, Piciullo L, Hefre H, Lacasse S (2021) Modelling of shallow landslides with machine learning algorithms. Geosci Front 12(1):385–393

Liu S, Wang L, Zhang W, Sun W, Fu J, Xiao T, Dai Z (2023) A physics-informed data-driven model for landslide susceptibility assessment in the Three Gorges Reservoir Area. Geosci Front 14(5):101621

Liu S, Wang L, Zhang W, Sun W, Wang Y, Liu J (2024) Physics-informed optimization for a data-driven approach in landslide susceptibility evaluation. J Rock Mech Geotech Eng 16(8):3192–3205

Liu S, Du J, Yin K, Zhou C, Huang C, Jiang J, Yu J (2024) Regional early warning model for rainfall induced landslide based on slope unit in Chongqing, China. Eng Geol 333:107464

Liu X, Shao S, Zhang C, Shao S (2025) Landslide susceptibility prediction in the loess tableland considering geomorphic evolution. Catena 249:108668

Lombardo L, Opitz T, Ardizzone F, Guzzetti F, Huser R (2020) Space-time landslide predictive modelling. Earth-Sci Rev 209:103318

Marin RJ, Velásquez MF, Sánchez O (2021) Applicability and performance of deterministic and probabilistic physically based landslide modeling in a data-scarce environment of the Colombian Andes. J South Am Earth Sci 108:103175

Marini F, Walczak B (2015) Particle swarm optimization (PSO). A tutorial. Chemometr Intell Lab Syst 149:153–165

Mathews NW, Leshchinsky BA, Mirus BB, Olsen MJ, Booth AM (2024) Regiongrow3D: a deterministic analysis for characterizing discrete three-dimensional landslide source areas on a regional scale. J Geophys Res Earth Surf 129(9):e2024JF007815

Medwedeff WG, Clark MK, Zekkos D (2025) Regional back-analysis of earthquake triggered landslide inventories: a 2D method for estimating rock strength from remote sensing data. J Geophys Res Earth Surf 130(1):e2023JF007471

Merghadi A, Yunus AP, Dou J, Whiteley J, ThaiPham B, Bui DT, Avtar Ram, Abderrahmane B (2020) Machine learning methods for landslide susceptibility studies: a comparative overview of algorithm performance. Earth-Sci Rev 207:103225

Mergili M, Marchesini I, Rossi M, Guzzetti F, Fellin W (2014) Spatially distributed three-dimensional slope stability modelling in a raster GIS. Geomorphology 206:178–195

Miao F, Wu Y, Xie Y, Li Y (2018) Prediction of landslide displacement with step-like behavior based on multialgorithm optimization and a support vector regression model. Landslides 15:475–488

Miao F, Wu Y, Török Á, Li L, Xue Y (2022) Centrifugal model test on a riverine landslide in the Three Gorges Reservoir induced by rainfall and water level fluctuation. Geosci Front 13(3):101378

Michel GP, Kobiyama M, Goerl RF (2014) Comparative analysis of SHALSTAB and SINMAP for landslide susceptibility mapping in the Cunha river basin, Southern Brazil. J Soils Sediments 14:1266–1277

Mirjalili S, Mirjalili SM, Lewis A (2014) Grey wolf optimizer. Adv Eng Softw 69:46–61

Montoya-Araque EA, Montoya-Noguera S, Lopez-Caballero F, Gatti F (2025) Numerical earthquake-induced landslide hazard assessment at regional scale in the Colombian Andes. Soil Dyn Earthq Eng 195:109370

Oguz EA, Depina I, Thakur V (2022) Effects of soil heterogeneity on susceptibility of shallow landslides. Landslides 19(1):67–83

Oliveira SC, Zêzere JL, Garcia RA, Pereira S, Vaz T, Melo R (2024) Landslide susceptibility assessment using different rainfall event-based landslide inventories: advantages and limitations. Nat Hazards 120(10):9361–9399

Ozbay A, Cabalar AF (2015) FEM and LEM stability analyses of the fatal landslides at Çöllolar open-cast lignite mine in Elbistan. Turk Landslides 12:155–163

Palazzolo N, Peres DJ, Bordoni M, Meisina C, Creaco E, Cancelliere A (2021) Improving spatial landslide prediction with 3d slope stability analysis and genetic algorithm optimization: application to the oltrepò Pavese. Water 13(6):801

Peláez JA, Hamdache M, Galindo-Zaldívar J, Henares J, Delgado J (2025) Landslide susceptibility assessment in the Rif-Tell orogenic belt region (NW Africa) from a PGA, PGV and AI probabilistic seismic hazard analysis. Soil Dyn Earthq Eng 195:109395

Peres DJ, Cancelliere A, Greco R, Bogaard TA (2018) Influence of uncertain identification of triggering rainfall on the assessment of landslide early warning thresholds. Nat Hazards Earth Syst Sci 18(2):633–646

Petley D (2012) Global patterns of loss of life from landslides. Geology 40(10):927–930

Pisner DA, Schnyer DM (2020) Support vector machine. Machine learning. Academic, pp 101–121

Pradhan B, Dikshit A, Lee S, Kim H (2023) An explainable AI (XAI) model for landslide susceptibility modeling. Appl Soft Comput 142:110324

Rashid B, Iqbal J, Su LJ (2020) Landslide susceptibility analysis of Karakoram highway using analytical hierarchy process and scoops 3D. J Mt Sci 17(7):1596–1612

Saadatkhah N, Mansor S, Kassim A, Lee LM, Saadatkhah R, Sobhanmanesh A (2016) Regional modeling of rainfall-induced landslides using TRIGRS model by incorporating plant cover effects: case study in Hulu Kelang, Malaysia. Environ Earth Sci 75:1–20

Salciarini D, Godt JW, Savage WZ, Baum RL, Conversini P (2008) Modeling landslide recurrence in Seattle, Washington, USA. Eng Geol 102(3–4):227–237

Schilirò L, Cevasco A, Esposito C, Mugnozza GS (2018) Shallow landslide initiation on terraced slopes: inferences from a physically based approach. Geomat Nat Hazards Risk 9(1):295–324

Suliman A, Zhang Y (2015) A review on back-propagation neural networks in the application of remote sensing image classification. J Earth Sci Eng 5(1):52–65

Sun G, Zheng H, Tang H, Dai F (2016) Huangtupo landslide stability under water level fluctuations of the three Gorges reservoir. Landslides 13:1167–1179

Tang L, Yu X, Jiang W, Zhou J (2023) Comparative study on landslide susceptibility mapping based on unbalanced sample ratio. Sci Rep 13(1):5823

Thiebes B, Bell R, Glade T, Jäger S, Mayer J, Anderson M, Holcombe L (2014) Integration of a limit-equilibrium model into a landslide early warning system. Landslides 11:859–875

Thomas J, Gupta M, Srivastava PK, Petropoulos GP (2023) Assessment of a dynamic physically based slope stability model to evaluate timing and distribution of rainfall-induced shallow landslides. ISPRS Int J Geo-Inf 12(3):105

Tran TV, Lee G, An H, Kim M (2017) Comparing the performance of TRIGRS and TiVaSS in spatial and temporal prediction of rainfall-induced shallow landslides. Environ Earth Sci 76(8):315

Tran TV, Alvioli M, Lee G, An HU (2018) Three-dimensional, time-dependent modeling of rainfall-induced landslides over a digital landscape: a case study. Landslides 15(6):1071–1084

den Van Bout B, Lombardo L, Chiyang M, van Westen C, Jetten V (2021) Physically-based catchment-scale prediction of slope failure volume and geometry. Eng Geol 284:105942

Van Westen CJ, Van Asch TW, Soeters R (2006) Landslide hazard and risk zonation—why is it still so difficult? Bull Eng Geol Environ 65:167–184

Vandromme R, Thiery Y, Bernardie S, Sedan O (2020) ALICE (assessment of landslides induced by Climatic Events): a single tool to integrate shallow and deep landslides for susceptibility and hazard assessment. Geomorphology 367:107307

Viet TT, Lee G, Thu TM, An HU (2017) Effect of digital elevation model resolution on shallow landslide modeling using TRIGRS. Nat Hazards Rev 18(2):04016011

Wang K, Zhang S, DelgadoTéllez R, Wei F (2019) A new slope unit extraction method for regional landslide analysis based on morphological image analysis. Bull Eng Geol Environ 78:4139–4151

Wang S, Zhang K, van Beek LP, Tian X, Bogaard TA (2020) Physically-based landslide prediction over a large region: scaling low-resolution hydrological model results for high-resolution slope stability assessment. Environ Model Softw 124:104607

Wang J, Xiao L, Zhang J, Zhu Y (2020b) Deformation characteristics and failure mechanisms of a rainfall-induced complex landslide in Wanzhou County, three Gorges Reservoir, China. Landslides 17(2):419–431

Wang J, Lu S, Wang SH, Zhang YD (2022) A review on extreme learning machine. Multimedia Tools Appl 81(29):41611–41660

Wang C, Zhou J, Wang Z, Yang Y, Lu J, Kang D, Wang Shaohua, Zhang H (2025) Assessment of landslide susceptibility in watersheds during extreme rainfall using a complex network of slope units. Sci Rep 15(1):5194

Woodard JB, Mirus BB (2025) Overcoming the data limitations in landslide susceptibility modeling. Sci Adv 11(8):eadt1541

Woodard JB, Mirus BB, Wood NJ, Allstadt KE, Leshchinsky BA, Crawford MM (2024) Slope unit maker (SUMak): an efficient and parameter-free algorithm for delineating slope units to improve landslide modeling. Nat Hazards Earth Syst Sci 24(1):1–12

Wu YM, Lan HX, Gao X, Li LP, Yang ZH (2015) A simplified physically based coupled rainfall threshold model for triggering landslides. Eng Geol 195:63–69

Xiao L, Wang J, Zhu Y, Zhang J (2020) Quantitative risk analysis of a rainfall-induced complex landslide in Wanzhou county, three Gorges reservoir, China. Int J Disaster Risk Sci 11(3):347–363

Xie N, Xin J, Liu S (2014) China's regional meteorological disaster loss analysis and evaluation based on grey cluster model. Nat Hazards 71:1067–1089

Xie W, Nie W, Saffari P, Robledo LF, Descote PY, Jian W (2021) Landslide hazard assessment based on bayesian optimization–support vector machine in Nanping City. China Nat Hazards 109(1):931–948

Xu C, Xu X, Yao X, Dai F (2014) Three (nearly) complete inventories of landslides triggered by the May 12, 2008 Wenchuan Mw 7.9 earthquake of China and their spatial distribution statistical analysis. Landslides 11:441–461

Xue Z, Feng W, Yi X, Dun J, Wu M (2024) Integrating data-driven and physically based landslide susceptibility methods using matrix models to predict reservoir landslides. Adv Space Res 73(3):1702–1720

Yan G, Liang S, Zhao H (2017) An approach to improving slope unit division using GIS technique. Sci Geogr Sin 37:1764–1770

Yang C, Liu LL, Huang F, Huang L, Wang XM (2023) Machine learning-based landslide susceptibility assessment with optimized ratio of landslide to non-landslide samples. Gondwana Res 123:198–216

Yang S, Tan J, Luo D, Wang Y, Guo X, Zhu Q, Ma Chuanming, Xiong H (2024) Sample size effects on landslide susceptibility models: a comparative study of heuristic, statistical, machine learning, deep learning and ensemble learning models with SHAP analysis. Computers & Geosciences 193:105723

Yu L, Wang Y, Pradhan B (2024) Enhancing landslide susceptibility mapping incorporating landslide typology via stacking ensemble machine learning in Three Gorges Reservoir, China. Geosci Front 15(4):101802

Zeng T, Gong Q, Wu L, Zhu Y, Yin K, & Peduto D (2024). Double-index rainfall warning and probabilistic physically based model for fast-moving landslide hazard analysis in subtropical-typhoon area. Landslides, 21(4), 753–773.

Zhang L, Ming D, Li Y, Cai J, Zhang Z (2024) A new slope unit extraction method based on terrain topology searching and vector similarity constraint for landslide analysis. CATENA 246:108355

Zhou C, Cao Y, Gan L, Wang Y, Motagh M, Roessner S, Hu Xie, Yin K (2024) A novel framework for landslide displacement prediction using MT-InSAR and machine learning techniques. Eng Geol 334:107497

Zhuang J, Peng J, Wang G, Iqbal J, Wang Y, Li W, Zhu X (2017) Prediction of rainfall-induced shallow landslides in the loess Plateau, Yan'an, China, using the TRIGRS model. Earth Surf Process Landforms 42(6):915–927